NTNU – Trondheim
Norwegian University of
Science and Technology

Analysis of Low-Frequency Damping in Mooring Lines for Floating Production Units

Eivind Tørset Magnussen

Marine Technology
Submission date: June 2014
Supervisor: Carl Martin Larsen, IMT
Co-supervisor: Erling Neerland Lone, DNV GL

Norwegian University of Science and Technology
Department of Marine Technology

NTNU Trondheim
Norwegian University of Science and Technology
Department of Marine Technology

MASTER THESIS, SPRING 2014

for

Stud.tech. Eivind Tørset Magnussen

Analysis of Low-Frequency Damping in Mooring Lines for Floating Production Units

(Analyse av lav-frekvent demping i ankerliner for flytende produksjonsanlegg)

Mooring analysis may be performed in a coupled or a de-coupled manner, and the choice is normally a compromise between accuracy and computational effort. De-coupled analysis is faster, and may in some cases provide satisfactory results. Coupled analysis is more time consuming, but takes into account the coupling effects between the vessel motion and the mooring lines. Low-frequency (LF) vessel motion has been shown to be largely influenced by current loading and damping due to the presence of mooring lines and risers. A good estimate of LF damping may therefore be crucial in order to achieve satisfactory results from a de-coupled analysis. Such an estimate may be obtained from a coupled analysis.

The main scope of the thesis will be to compare results from coupled analysis and de-coupled analysis using damping estimates from the coupled analysis. This should be performed through a case study on a turret-moored FPSO with catenary lines at 320m water depth.

The thesis may be summed up as:

1. Perform a literature study and present the theories most relevant to the case study.

2. Establish a coupled model.

3. Establish the short-term distributions from one or several points on a 100-year contour line.

4. Choose two conditions (extreme and moderate storm) and estimate the damping coefficient.

5. Perform a de-coupled analysis with the damping coefficient in pt. 4 as input.

6. Compare results from coupled and de-coupled analysis. The comparison should involve:
   a. Mean values.
   b. Standard deviations.
   c. Maximum values.
   d. Time series of surge motion and line force
   e. Extreme value distribution (from seed variation).

If time permitted, sensitivity studies may be performed, e.g.:

7. Sensitivity in the damping estimate from:
   a. Seed variation.
   b. Simulation length.
   c. Alternative heading
   d. Current velocity and/or profile.

8. Sensitivity in the de-coupled analysis from various damping levels.

Additional analyses might also show to be of interest during the work

The work may show to be more extensive than anticipated. Some topics may therefore be left out after discussion with the supervisor without any negative influence on the grading.

The candidate should in her/his report give a personal contribution to the solution of the problem formulated in this text. All assumptions and conclusions must be supported by mathematical models and/or references to physical effects in a logical manner. The candidate should apply all available sources to find relevant literature and information on the actual problem.

The report should be well organised and give a clear presentation of the work and all conclusions. It is important that the text is well written and that tables and figures are used to support the verbal presentation. The report should be complete, but still as short as possible.

The final report must contain this text, an acknowledgement, summary, main body, conclusions and suggestions for further work, symbol list, references and appendices. All figures, tables and equations must be identified by numbers. References should be given by author name and year in the text, and presented alphabetically by name in the reference list. The re-port must be submitted in two copies unless otherwise has been agreed with the supervisor.

From the report it should be possible to identify the work carried out by the candidate and what has been found in the available literature. It is important to give references to the original source for theories and experimental results. The report should be delivered according to instructions from the faculty, and - if needed – additional material (binder, VD/CD/memory stick) should be delivered to the supervisor.

The work will be carried out in cooperation with DNV GL

Contact person at DNV GL Erling Neerland Lone

Deadline: June 10th, 2014

Carl M. Larsen
Supervisor

Preface

The work for this master thesis has been carried out at the Department of Marine Technology, at the Norwegian University of Science and Technology (NTNU) during the spring of 2014. It has been carried out in cooperation with Det Norske Veritas GL (DNV GL) under the supervision of Prof. Carl M. Larsen, and under co-supervision of M.Sc Erling N. Lone from DNV GL in Trondheim.

I would like to thank my supervisor Prof. Carl M. Larsen for scheduling regular meetings, and for his help and guidance during the thesis work.

Many thanks go out to my co-supervisor Erling N. Lone, who's help and insight has been vital for the progress of this thesis. I am grateful that he has taken time out of his working hours to provide lectures and valuable discussions, shown great support and interest in the work, and been available whenever I had questions or problems. DNV GL is acknowledged for allowing him to do so during his working hours. Erling is also acknowledged for providing the necessary input files and filtering routines

Lastly, I would like to thank my fellow students at the office for valuable discussions, and for providing feedback on the report.

Eivind T. Magnussen,
Trondheim, Tuesday 10^{th} June, 2014

Summary

In this thesis, the relationship between mooring line damping and system responses, due to varying environmental conditions, is investigated. The responses focus mainly on the low-frequency (LF) components and on the modelling capabilities of coupled and uncoupled analysis.

Moored vessels are exposed to time varying environmental loads, such as wind, waves and current, which give rise to large dynamic motions. The presence of mooring introduces a low stiffness and a high natural period in the horizontal plane. Due to second order difference frequency effects, one will get a low frequency resonant excitation from the waves. This effect is enhanced by the slowly varying wind force. The total dynamic response will therefore be due to a combination of the first order wave frequency (WF) motion and of the resonant low frequency (LF) motion. The LF motion requires an accurate assessment of the damping in the system, and mooring lines will in many cases constitute a large portion of the damping.

The dynamics of mooring lines can be analysed by different methods and one usually distinguish between frequency domain (FD) and time domain (TD) calculations, and between coupled and uncoupled analysis. The choice of method is usually a compromise between accuracy and computational effort, where a non-linear coupled simulation in TD will yield the most accurate results. The goodness of the results depends largely on the system, and approximate methods such as FD and uncoupled analysis must be handled with great care, as the accuracy of the results may be dissatisfactory.

Coupled and uncoupled analysis models of a turret-moored FPSO at 320 meters water depth are established, and calculations are performed in TD. Damping from mooring lines are estimated from coupled analyses and applied to the corresponding uncoupled model as linear vessel damping coefficients. Mean current forces are also estimated from coupled analyses, and applied as constant forces acting on the vessel. Model applicability and limitations are discussed through a comparison of coupled and uncoupled results.

The main case investigated is an extreme 100-year storm with head sea conditions. Parameter studies are also performed, in order to study the effect on the damping estimate and on the responses. Among these are a seed variation of the main case, a less severe condition with reduced peak period and significant wave

height, an alternative current profile, an alternative heading, and a damping sensitivity study.

The uncoupled model show a good agreement with the coupled model for the less severe condition. Discrepancies become more apparent as the current velocity is increased, or as WF motions becomes more prominent. This is because the uncoupled model uses a linear coefficient to represent the damping in the mooring lines, while in the coupled model the correct non-linear damping contributions from the lines are automatically included. The discrepancies caused by introducing such a linear coefficient becomes larger as the damping level increases. Both current velocity and WF excitation will increase the damping contribution from the mooring lines.

Reducing the peak period and wave height results in a decrease in WF response and damping estimate. This confirms that WF motion is an important contributor to the damping in mooring lines. WF motion decreases both because of lower values in the first order transfer functions, and because the energy in the wave spectrum is proportional to the wave height and to the square of the peak period. Contrary to the WF motion, LF motion increases when the peak period is reduced, because of higher values in the drift coefficients. The increase in drift coefficient values outweighs the effect from a reduction in spectral energy.

Interestingly, a reduction in peak period increases both the resonant LF motion and the accuracy in the uncoupled results. The accuracy in LF motion is greater, despite an increase in motion magnitude, because the overall damping is reduced. Therefore, an increase in LF motion does not itself necessarily lead to an increased sensitivity, or a poorer representation of this motion in the uncoupled model.

Results from the sensitivity study show that a low uncertainty in the mooring line damping estimates may lead to large or moderate uncertainties in the LF response, and by consequence in the total response. Extreme response is affected through the uncertainties of the LF response, as LF constitutes a large portion of the total response. This confirms that the LF response is highly sensitive to mooring line damping. Accurate estimates are need for both LF and extreme response.

Sammendrag

I denne oppgaven blir forholdet mellom demping i ankerliner og systemrespons, på grunn av varierende miljøforhold, undersøkt. Resultatene fokuserer hovedsakelig på de lavfrekvente (LF) komponentene, og på modellerings-egenskapene til koblet og ukoblet analyse.

Forankrede fartøy vil, pga. tidsvarierende miljølaster som vind, bølger og strøm, kunne oppleve store dynamiske bevegelser. Ankerlinene bidrar til en lav stivhet i horisontalplanet, samt en høy naturlig periode, og på grunn av andreordens effekter fra differansefrekvenser vil man få en lavfrekvent (LF) resonans-bevegelse. Denne effekten forsterkes av den langsomt varierende vindkraften. Den totale dynamiske responsen vil derfor være en kombinasjon av førsteordens bølgefrekvent (WF) bevegelse og den resonante LF-bevegelsen. LF bevegelsen krever en nøyaktig vurdering av den totale dempingen i systemet, og ankerlinene vil i mange tilfeller utgjøre en stor del av denne dempingen.

Dynamikken i forankringslinene kan analyseres ved forskjellige metoder, og man skiller vanligvis mellom løsningsmetoder i frekvensdomene (FD) og tidsdomene (TD), samt mellom koblet og ukoblet analyse. Valg av metode styres vanligvis av et kompromiss mellom nøyaktighet og beregningstid, hvor en ikke-lineær koblet simulering i TD vil gi de mest nøyaktige resultatene. Godheten av resultatene avhenger av system, og for forenklede metoder som FD og ukoblet analyse må håndteres med stor forsiktighet, da de kan føre til resultater med utilstrekkelig nøyaktighet.

Koblede og ukoblede analysemodeller av en turret-forankret FPSO på 320 meters vanndyp er etablert, og beregningene utføres TD. Demping fra ankerlinene estimeres fra koblede analyser, og anvendes på den tilsvarende ukoblede modellen som lineære dempningskoeffisienter på fartøyet. Midlere strømkrefter estimeres også fra koblede analyser, og påføres som konstante krefter på fartøyet i den ukoblede modellen. Modellbegrensninger diskuteres gjennom en sammenligning av koblede og ukoblede resultater.

Hovedkondisjonen som undersøkes er en kraftig 100års-storm i motsjøtilstand. Parameterstudier blir også gjennomført, for å studere virkningen på dempningsestimatet og på responser. Blant disse er frøtallsvariasjon av hovedkondisjonen, en mer moderat 100års-storm med redusert Hs og Tp, et alternativt strømprofil, en alternativ fartøysvinkel, og en sensitivitetsstudie av dempingsestimatet.

Resultatene fra ukoblede analyser samsvarer godt med de koblede analysene, for den mest moderate miljøkondisjonen. Avvik blir mer synlige etter hvert som strømhastigheten økes, eller når bølgefrekvente (WF) bevegelser blir mer fremtredende. Dette er fordi den ukoblede modellen benytter seg av lineære koeffisienter til representere dempningen i ankerlinene, mens det korrekte ikke-lineære dempingsbidraget fra linene automatisk inkluderes i den koblede modellen. Feilen som oppstår ved å innføre slike lineære dempingskoeffisienter blir større etter hvert som dempningsnivået øker. Både strømhastighet og WF bevegelse vil bidra til å øke dempingen i forankringslinene.

En reduksjon i bølgespekterets topp-periode og i signifikant bølgehøyde fører til en reduksjon i bølgefrekvent respons og dempingsestimat. Dette bekrefter at demping fra ankerliner i stor grad påvirkes av den bølgefrekvente bevegelsen. Denne bevegelsen avtar både på grunn av lavere verdier i førsteordens transferfunksjon, og på grunn av at energien i bølgespektereter er proporsjonal med signifikant bølgehøyde, og med kvadratet av topp-perioden. I motsetning til WF bevegelse, øker LF bevegelse når topp-perioden reduseres. Dette skjer på grunn av høyere verdier i andreordens driftskoeffisienter. Økningen i driftskoeffisientverdier veier opp for en reduksjon i spekterenergien.

Det er verd å merke seg at en reduksjon i bølgespekterets topp-periode vil både øke LF bevegelse og minke forskjellene mellom koblet og ukoblet analyse. En økning i LF bevegelse vil derfor ikke nødvendigvis i seg selv føre til en økt følsomhet for demping, eller en dårligere representasjon av denne bevegelsen i den ukoblede modellen.

Resultater fra følsomhetsstudiet viser at en lav usikkerhet i dempings-estimatet kan føre til store eller moderate usikkerheter i LF respons, og dermed også i den totale responsen. Ekstremresponsen påvirkes gjennom usikkerheten til LF respons, ettersom LF respons utgjør en stor del av denne. Dette bekrefter at LF bevegelsen er svært følsom for demping i ankerliner, og at nøyaktige estimater derfor er nødvendig for både lavfrekvent og ekstrem respons.

Contents

Nomenclature

General comments

- Symbols and abbreviations are generally defined the first time they appear in the text.
- Only the most used symbols are defined here.
- Matrices and vectors are denoted by using bold face, e.g. $\mathbf{M}$ or $\mathbf{x}$.
- Superscript dots denotes differentiation w.r.t. time, e.g. $\dot{x} = \frac{dx}{dt}$, $\ddot{x} = \frac{d^2x}{dt^2}$
- A symbol may be given several meanings.

Abbreviations

COG	Center Of Gravity
CV	Coefficient of Variation
DNV GL	Det Norske Veritas Germanischer Lloyd
DOF	Degree(s) Of Freedom
FD	Frequency Domain
FEM	Finite Element Method
FPSO	Floating Production, Storage and Offloading
LF	Low Frequency
STD	Standard deviation
TD	Time Domain
WF	Wave Frequency

Symbols

B_{ij}	Linear damping component in DOF ij
$\mathbf{C}$	Damping matrix
C_i	Current force coefficient
C_d	Drag coefficient
C_i^{WD}	Wave-drift coefficient
c_n	Stochastic amplitude or linear damping estimate

$\mathbf{D}_{1,2}$	Linear and quadratic vessel damping matrix
E[ ]	Expected value
EA	Axial stiffness
$\mathbf{F}$	Force vector
H(ω, β)	First order transfer function as a function of wave frequency and heading
H_S	Significant wave height
$\mathbf{K}$	Stiffness matrix
$\mathbf{M}$	Mass matrix
$\mathbf{q}$	General load vector
r	General structural response
S	Spectral density
T	Axial tension
T_P	Spectral peak period
$\mathbf{x}$	3-DOF (surge, sway, yaw) or 6-DOF position vector
x_T	Distance between COG and turret center

α	Heading or Gumbel parameter
β	Wave direction or Gumbel parameter
ϵ	Error or stochastic phase angle
ζ	Wave elevation
Θ	General variable
μ	Frequency difference, $\omega_j - \omega_i$
σ_x	Standard deviation of x
ϕ	Phase angle between load and response
ω	Circular wave frequency

Subscripts and Superscripts

$\hat{x}$	Approximation of x
$\bar{x}$	Average value of x
x_a	Amplitude of x
x^{LF}	Low frequency component of x
x^{WF}	Wave-frequency component of x
x_e	Expected 3-hour maximum value of x
x_s or x^s	Static value of x
x_d	Dynamic value of x
x_{mo}	Component of x due to mooring loads
x_{wa}	Component of x due to wave excitation
x_{wi}	Component of x due to wind excitation
x_c or x^c	Component of x due to current

List of Figures

List of Tables

Chapter 1

Introduction

1.1 Background

Moored vessels are exposed to time varying environmental loads, such as wind, waves and current, which give rise to large dynamic motions. The presence of mooring introduces a low stiffness in the horizontal plane and a high natural period. Due to second order difference frequency effects one will get a low frequency resonant excitation. This effect is enhanced by the slowly varying wind force. The total dynamic response will therefore be due to a combination of the first order wave frequency (WF) motion and of the resonant low frequency (LF) motion. LF motion requires an accurate assessment of the damping in the system, and mooring lines will in many cases constitute a large portion of the damping. Acquiring accurate estimates of the mooring line damping is however, not a trivial task. Both stiffness and drag loads on the mooring system are non-linear, which complicates the process.

The dynamics of mooring lines can be analysed by different methods, and one usually distinguish between frequency domain (FD) and time domain (TD) calculations, and between coupled and uncoupled analysis. The choice of method is usually a compromise between accuracy and computational effort, where a non-linear coupled simulation in time domain will yield the most accurate results. The quality of the results largely depend on the system, and approximate methods such as FD and uncoupled analysis must be handled with great care, as the accuracy of the results may be unsatisfactory. The choice will also depend on the objective of the analysis. For severe sea states, accurate methods may be required as non-linearities may not be adequately accounted for by simplified formulations.

The objective of a mooring analysis is usually to obtain statistical measures for vessel motion and mooring line forces, allowing an assessment of riser tolerance, as well as fatigue and extreme loads in the mooring lines.

As the LF excitation is a resonant motion, accurate damping estimates may be necessary in order to sufficiently capture the realistic motions, when utilizing approximate methods. Using approximations or neglecting mooring line damping completely often leads to over-conservative estimates of vessel motions and line tension.

Uncoupled procedures are generally unable to capture the mooring line damping with sufficient accuracy, which in deep waters or in areas with large current may constitute a significant part of the total damping, as reported by Ormberg et al. (1997), Low and Langley (2007) and Webster (1994).

A coupled analysis captures the mooring line damping and drag forces automatically through an iteration scheme, where the equilibrium configuration for each time step is established. However, the computational effort needed to undergo such an analysis is still too great to be used in early design phases. An uncoupled analysis on the other hand is faster, but relies on approximations of the damping and drag forces during vessel response calculations. Different approximations have been developed for both frequency domain (FD) and time domain (TD).

1.2 Scope

The purpose of this thesis is to study the relationship between mooring line damping and the system responses, due to varying environmental conditions. In particular, the low-frequency (LF) offset and tension is of interest, due the resonant nature of the motion. The applicability of the proposed estimation technique for mooring line damping is also investigated. Their results focus mainly on the effect of the environmental conditions on the damping estimates and the responses, and on the uncertainty in the damping estimates. Its effect on the low-frequency component, and on the modelling capabilities of coupled and uncoupled analysis, is also considered. For this purpose, a turret moored FPSO at 320m water depth in severe sea states is used, and calculations are performed in time domain (TD) by the Marintek softwares SIMO, RIFLEX and SIMA, the latter being a graphical interface which also enables communication between SIMO and RIFLEX. Seed variations, additional environmental conditions, and a damping sensitivity study is also performed.

1.3 Thesis Structure

Chapter 2 gives a brief outline of theories and methods of analysis related to the case study and mooring analysis in general. The focus is on descriptions, limitations and advantages.

Chapter 3 discusses different damping contributions that are important for a moored ship-shaped floater.

Chapter 4 present the software utilized in the case study, and their theoretical backgrounds.

Chapter 5 gives a description of the case studies, including vessel particulars, environmental conditions and mooring configuration.

Chapter 6 presents the model specific theories, and outlines the procedure for estimating mooring line damping, as well as mean current forces, from a coupled simulation.

Chapter 7 presents and discusses the results with reference to theory presented in previous chapters.

Finally, chapter 8 and 9 presents the conclusions drawn from the discussions, and give some suggestions to further work.

Chapter 2
Stochastic Analysis

In this section, the most important analysis methods related to the case study are presented, such as time domain (TD) and frequency domain (FD) calculations, as well as coupled and uncoupled analysis. The focus is on the methodology, their advantages, and their limitations, which will later be used to explain differences in results. Methods for calculating wave-frequency (WF) and low frequency (LF) responses, as well as the dynamic behaviour of these responses, are outlined and discussed. The focus of the responses are on statistical parameters and statistical uncertainty, as well as their connection to the line damping estimates. In addition, a method for establishing extreme response statistics, is a briefly outlined.

2.1 Frequency and Time Domain

The two main calculation methods used in stochastic analysis today are frequency domain (FD) and time domain (TD). Both calculation methods have their advantages and limitations, which in the following sections will be discussed.

Time domain simulations are performed in the case study. However, a short outline of the frequency domain methodology is first presented to provide a basis for comparison.

2.1.1 Frequency Domain

The frequency domain (FD) calculations are based on the principle of linear superposition, where the total response is taken as the sum of responses found from each wave frequency component. The stochastic process is described by power spectra, and for a Gaussian process these spectra give a complete description of the statistical properties. This means that the results will not contain any statistical uncertainty. The model uncertainties however, may be quite substantial.

The response spectra are found by a combination of the wave power spectra and the corresponding transfer functions.

The assumption of a Gaussian process is normally acceptable for WF responses, but LF surge motion will in reality have a distribution that lies somewhere between a Guassian and an exponential, while the LF line tension is usually more or less exponentially distributed (Lie, 2013). The response is calculated for one frequency at a time, and in order to obtain the full spectra, the spectrum equations must be solved for a range of frequencies.

FD calculations for a system with many degrees of freedom can get quite complex (Magnussen, 2013). A motivation for performing these calculations, is that once the spectra have been established, these can be used to derive statistical properties, which in turn can be used in estimation of fatigue damage. Under a Gaussian assumption, the wave heights will be Rayleigh distributed, and the expected extreme response can be estimated fairly easily as well.

It is important to note that if the load can not be represented as sum of harmonic functions, or if the principle of linear superposition does not hold, then FD analysis cannot be performed. The method may also give poor results for systems with large non-linear effects.

The main advantages of FD analysis is that they are generally very fast compared to TD simulations, and that it is possible to include frequency dependent added mass and damping. One drawback is that these methods rely on linear equations, and hence requires a simplification of the non-linear damping and stiffness forces. This inevitably causes inaccuracies in the results. Several linearisation methods have been developed in order to minimize these mentioned inaccuracies. Methods such as harmonic and stochastic/statistical linearisation, as described by Low and Langley (2007) and Rodenbusch et al. (1986), are often used in the litterature. Some limitations in these are discussed in connection with coupled and uncoupled analysis (Section 2.2). FD calculations may be used for moderate sea state, which constitute the largest contribution to fatigue damage, as the non-linearities may be satisfactory accounted for by simplified formulations (Lone, 2009). For severe sea states, however, the non-linearities may be too great, and in such cases a time domain approach is preferred.

2.1.2 Time domain

Time domain (TD) simulations are performed through stepwise time integration of the dynamic equilibrium equation, which usually calls for numerical procedures like the Newmark-β family. Unlike in FD procedures, the excitation may

be random. Damping and stiffness terms may be updated during these numerical procedures, and hence non-linear effects may be included (Langen and Sigbjornsson, 1979). TD simulations are the most frequently used methods for calculation of dynamic response in slender marine structures today. The reason is that most shortcomings associated with FD analyses, such as incorrect representation of non-linear drag force, forces in the splash zone, transient motion and mooring stiffness, which are important for such structures, can easily be accounted for in TD (Lone, 2009). TD simulations are performed by generating random time series of the surface elevation, based on statistical properties obtained from the wave spectra. These time series may be generated by an inverse Fourier transform in different ways. Two common ways are by means of stochastic amplitude and phase, and by deterministic amplitudes and stochastic phase. In the latter case the Fourier transform will follow the equation:

$$\zeta(t) = \sum_{n=1}^{N} c_n \sin(\omega_n t - \varepsilon_n) \tag{2.1}$$

where the component amplitude c_n is deterministic and given from the auto spectrum according to

$$c_n = \sqrt{2S_x(\omega_n)\Delta\omega_n} \tag{2.2}$$

The phase angle ε_n is an independent stochastic variable taken from an even distribution in the interval [0,2π]. The time series will, when using this method, have a variance equal to to the area of the auto spectrum. This is not the case for a sample of limited length taken from a Gaussian process. Thus, the samples generated by this method will not represent a true Gaussian process. This will in turn affect the distribution of extremes, and give a difference in grouping effects for individual maxima, which might be important in reliability analysis. The method will however, give a correct distribution for individual maxima (Larsen, 2013).

In the case of stochastic amplitude and phase it is possible to generate samples with correct statistical properties. The c_n in Eq. (2.1) is then a stochastic variable given by:

$$c_n = \sqrt{a_n^2 + b_n^2} \tag{2.3}$$

where a_n and b_n are Gaussian distributed stochastic variables with identical parameters. c_n will then be Rayleigh distributed with variance equal to to sum of variances for the two components. c_n can be related to the auto spectrum through the following relationship:

$$c_n = \sqrt{-ln(1-r)}\sqrt{2S_x(\omega_n)\Delta\omega_n} \tag{2.4}$$

where r is a random number taken from an even distribution in the interval [0,1].

TD simulations may contain large statistical uncertainties since the surface elevation is generated as random time series. This is especially true for large wave heights, which are more rare. Because large wave heights are such rare events, the duration of the simulation must be increased in order to get good estimates of extreme responses. Sufficient simulation length is also important to ensure for LF responses, as these cyclic responses have much larger periods than WF repsonses. The duration may be increased by either prolonging one simulation, or by running several shorter simulations with different surface realizations.

The main drawbacks of TD simulations are that they are much more time consuming than FD calculations, and that the results contain statistical uncertainties. In addition, the added mass and damping is generally frequency dependent. In TD they can either be Fourier transformed to give the so called retardation functions, or they can be treated in a more approximate way by using a fixed value chosen at a representative frequency (Low and Langley, 2007).

2.1.3 Frequency vs. time domain

Both methods discussed have their advantages and disadvantages. These will have to be considered before performing an analysis. Requirements on accuracy, computational effort, and degree of non-linearities in the system will often determine the choice of method. The most important properties of these methods are listed in Table 2.1

Table 2.1: Properties of frequency domain and time domain

Frequency domain	**Time domain**
Advantages	
Low computational cost	Non-linearities included
No statistical uncertainty	Transient response
Frequency dependent added mass and damping	
Disadvantages	
Requires linearisation	Statistical uncertainty, i.e several simulations are required
Only steady-state response	High computational cost

2.2 Coupled and Uncoupled analysis

FD and TD analyses may be performed either in a coupled or an uncoupled manner, and one often differentiate between two types of couplings: one between

vessel and slender structures, and the other between mean offset, and the WF and LF motion. A coupled analysis is here referred to an analysis where both these couplings are preserved.

While coupled analysis is able to capture the current loads and damping contribution from mooring lines and risers more accurately, uncoupled analysis requires simplifications of these contributions. For a fully non-linear analysis, a coupled analysis in TD is required. Thorough descriptions of coupled and uncoupled analysis in time domain and frequency domain are given in the literature, see e.g. Garrett (2005), Ormberg and Larsen (2004), Low and Langley (2007), and Ormberg et al. (1998).

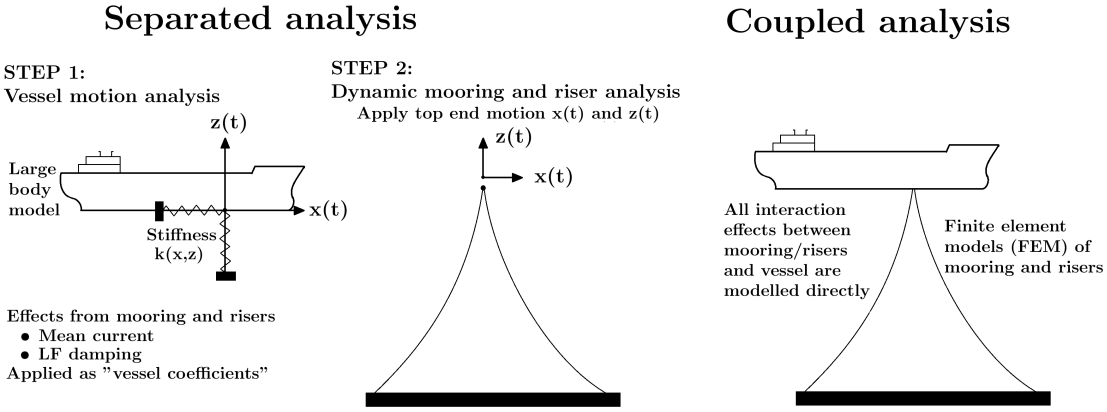

Figure 2.1: Coupled and uncoupled analysis (Ormberg and Larsen, 2004)

2.2.1 Uncoupled Analysis

Uncoupled analysis is usually executed in two steps, as shown in Figure 2.1. These steps can be summed up in the following way:

1. Calculate vessel motions with simplified or neglected influence from mooring lines.

2. Perform dynamic response analysis for mooring and risers, using the motion response from step 1 as top end excitation.

In step 1, WF and LF motions are calculated for the vessel, e.g. by the methods described in Sections 2.3 and 2.4. Load effects from mooring lines are modelled quasi-statically as position-dependent forces, i.e. as stiffness contributions. These stiffness contribution are usually denoted as line characteristics, and depends on

both elastic and geometrical stiffness properties in mooring line. This will be further elaborated in the subsequent sections. In the uncoupled approach two simplifications are usually made:

1. The damping forces from mooring lines are either neglected or implemented in a rough manner as a linear damping force acting on the vessel

2. The stiffness contribution from current on the mooring lines are either neglected or incorporated as an additional current forces acting on the vessel.

The former simplification may significantly affect the LF motion, as damping contribution from mooring often constitute a major part of the total system damping. The latter simplification implies that either the horizontal turret forces and line tensions, or the mean offset may be inaccurate (Ormberg and Larsen, 2004). This depends on whether the current force is included or neglected, where neglecting the current force will lead to an incorrect offset. Both the linear damping force and the mean current force must be estimated by separate programs or methods, and given as additional coefficients or forces on the vessel during step 1 of the analysis.

Step 2 is the time consuming part of an uncoupled analysis, as it often involves non-linear finite element calculations (FEM). Consequently, the calculations are normally only carried out on critically loaded lines, one by one.

Due to the simplifications discussed above, the model will have certain shortcomings. The mean current loads on moorings and risers will usually not be accurately accounted for. This particularly applies to deeper water and on systems with many risers (more drag), as the interaction between the current forces on the moorings and risers, and mean offset and LF motions of the vessel is larger. Furthermore, since the damping effect from moorings and risers is affected by WF motions on the line, simplifications of the damping force is not necessarily straight forward. This is because WF motions itself requires comprehensive computation. A good estimate of LF damping is necessary in order to get accurate results from uncoupled analysis (Ormberg and Larsen (2004); van den Boom (1985))

2.2.2 Coupled Analysis

In coupled analysis, the vessel motion and the dynamic response on mooring lines and risers are obtained simultaneously, as shown in Figure 2.1. As a result, the full interaction between mooring, riser and vessel response is taken into account.

The main objective of performing a coupled analysis is to get better accuracy in mean offset and LF motions. This is achieved by including mean current forces on the mooring lines, and by proper estimates of the LF damping. This becomes increasingly important as water depth increases, due to the limitations in the uncoupled model.

Because of the computational effort required in a coupled time domain analysis, the application might be limited to study a few important load cases, establishing reliable estimates of LF damping and mean current forces, and to verify studies and models where limited basin depth make models test impossible. Coupled analysis requires that the complete mooring and riser system is included in the model.

2.2.3 Coupling Effects

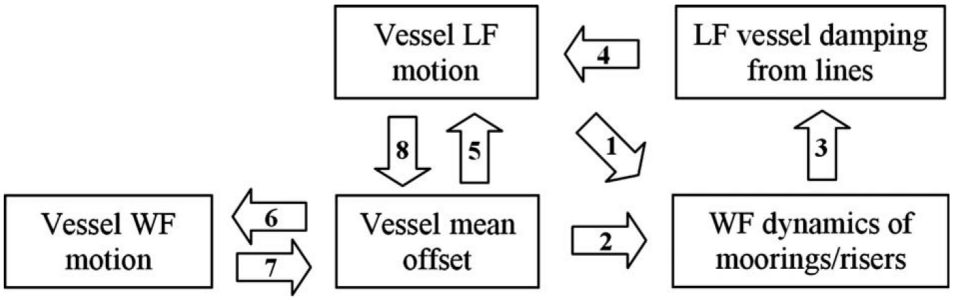

Figure 2.2: Coupling effects in a mooring analysis (Low and Langley, 2008*b*)

As previously mentioned, there are two types of couplings: one between vessel and slender structure (type 1), and one between the mean offset, and the WF and LF motion (type 2). In the following, several of these couplings are identified and described. For a more thorough description reference is made to Low and Langley (2008*b*).

The mean offset and LF motion constitute significant contributions to the total offset, and may in extreme cases constitute up to 95% in deep water. This value decreases to 50% in 70 m water depth (Low and Langley, 2008*b*). The total offset determines the mooring line configuration, and in turn the WF dynamics of the lines. Hence, the mean offset and LF motion affects the WF dynamic, as indicated by arrows 1 and 2 in Figure 2.2.

The total damping is largely influenced by line drag, in which WF dynamics are a dominant part (LF velocities are small). As LF motion is essentially a resonant motion, it is especially sensitive to the total damping. Hence, the WF dynamics affects the LF motion through damping, as indicated by arrows 3 and 4.

There are also coupling effects that arises from the non-linear stiffness characteristics of a system. The mean offset largely determines the tangential stiffness in the system, and therefore the vessel motion. This is because a larger mean offset increases the stiffness, as shown in the restoring characteristics (Figure 2.7). As a consequence, the motion generally becomes more restricted. These couplings are indicated by arrows 5 and 6.

In addition, the non-linearity of the restoring characteristic creates a *setdown* effect. Setdown is created by an asymmetric oscillation about the static offset $\bar{X}_S$. This is because the non-linear nature of the restoring characteristic will restrict the movement more to one direction than the other, as indicated in Figure 2.3. This creates a dynamic mean offset $\bar{X}_D$ which is different from the static offset, $\bar{X}_s$, and the *setdown* is defined as the difference between the static and the dynamic mean offset. In general, oscillations will decrease the mean offset, and the magnitude of the setdown will be influenced by the extent of vessel motion. This coupling is indicated by arrows 7 and 8.

Compared to a stationary body, the mean current forces are larger on an oscillating body, due to the non-linearity of drag. The consequence is a tendency to increase the mean offset, denoted as *setup*. The setdown from non-linear restoring, and *setup* from non-linear drag are concurrent effects, and whether the overall mean offset increases or decreases depends on the system.

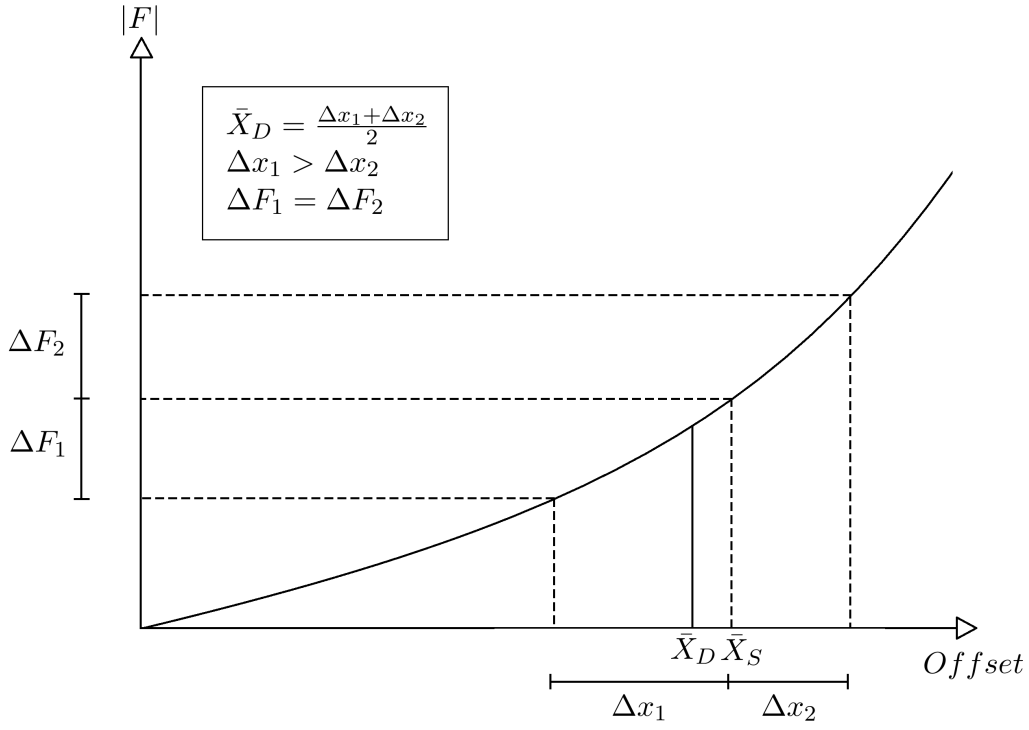

Figure 2.3: Setdown

From the above discussion, it is seen that type 2 coupling depends on the degree of non-linearity in the system, and would be absent in the case of a linear restoring characteristic. Type 2 coupling is particularly prevalent in shallow water, as the non-linearity in the restoring forces are greater (Low and Langley, 2008*b*).

2.3 Wave Frequency (WF) Response

2.3.1 WF Motion

Due to the negligable effect from high frequency wind forces, the wave-frequency motion is mainly excited by first order wave forces. Hence the linear equation of motion may be written as

$$\mathbf{M}(\omega) \cdot \ddot{\mathbf{x}}^{WF} + \mathbf{C} \cdot \dot{\mathbf{x}}^{WF} + \mathbf{K} \cdot \mathbf{x}^{WF} = \mathbf{F}_{wa}^{WF} \tag{2.5}$$

where $\mathbf{M}(\omega)$ is the mass matrix including frequency dependent mass, $\mathbf{C}$ is the damping matrix, $\mathbf{K}$ is the stiffness matrix and $\mathbf{F}_{wa}^{WF}$ is the first order wave excitation force. Eq. (2.5) can be solved in either time domain (TD) or frequency

domain (FD) as described in Section 2.1. In the former method, the equation can be modified to account for non-linearities as well.

In frequency domain, Eq. (2.5) is solved through:

$$S_{xi}^{WF}(\omega) = \int_0^\infty |H_i(\omega,\beta)|^2 \cdot S_{\zeta\zeta}(\omega,\beta)d\beta \quad i = 1, ...6 \tag{2.6}$$

where S_{xi}^{WF} is the WF response spectrum, $H_i(\omega,\beta)$ is the first order transfer function and $S_{\zeta\zeta}$ is the wave spectrum, which depends on the heading, β, and the frequency, ω, of the wave component.

The WF vessel motions will, due to large displacements, normally not be affected by the mooring forces, and hence the contribution from mooring lines are not included in the damping and stiffness matrices (van den Boom, 1985).

2.3.2 WF Tension

WF tension can usually be calculated in two ways:

1. Quasi-statically, as a function of fairlead position, by neglecting dynamic forces.

2. Dynamically, accounting for inertia and drag forces on line.

Due to an eccentricity between the fairleads and the vessel's center of gravity, and due to coupling between different directions, the fairleads will experience large dynamic motions. For a turret moored FPSO, this coupling is mainly between surge, heave and pitch. An example of typical fairlead motion is shown in Figure 2.4. The figure shows that the top end moves in an elliptic manner, and how this causes large dynamic motions. This is particularly true for leeward lines. At a point further away from the vessel's center of gravity, the minor axis on the ellipse, as well as the angle between the major axis and the horizontal plane, will decrease.

Due to the large rapid motion, the tension response should ideally be solved dynamically. This is often done with a finite element model (FEM), as the effects of drag and inertia can easily be implemented.

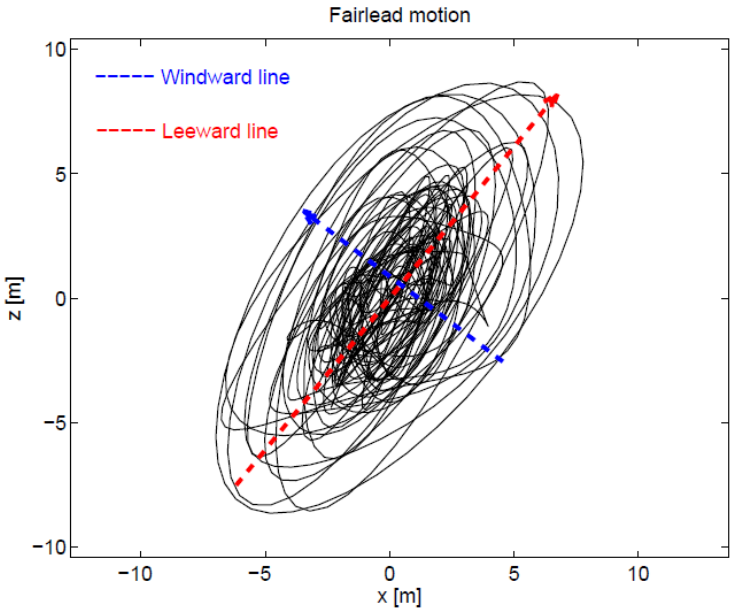

Figure 2.4: Typical fairlead motions for waves propagating along the negative direction of the $x-axis$ (Lone, 2009)

2.4 Low Frequency (LF) Response

2.4.1 LF motion

LF motion is a resonant motion excited by a slowly varying drift force, caused by a combination of slowly varying wind and second order difference frequency wave forces. Hence, the non-linear equation of motion can be expressed as:

$$\mathbf{M}(\omega) \cdot \ddot{\mathbf{x}}^{LF} + \mathbf{C}(\dot{\mathbf{x}}) \cdot \dot{\mathbf{x}}^{LF} + \mathbf{K}(\mathbf{x}) \cdot \mathbf{x}^{LF} = \mathbf{F}_{wa}^{LF} + \mathbf{F}_{wi}^{LF} \tag{2.7}$$

where $\mathbf{F}_{wa}^{LF}$ and $\mathbf{F}_{wi}^{LF}$ are the slowly varying drift forces from waves and wind, respectively. For LF motion, forces from the mooring system are important and must be included in the damping and stiffness matrices. This makes them non-linear, as the contribution from mooring damping and stiffness depends on the instantaneous top end position and velocity.

The non-linearity of the stiffness matrix is easily accounted for in time domain, as it may be updated for each time step. Inclusion of the damping forces, however, depends on the mooring line model used.

In FD calculations these non-linearities are not easily accounted for, as explained in Section 2.1.1. In addition, the quadratic transfer functions are approximated

by drift coefficients, a method knowns as *Newman's approximation*. The application of this approximation is acceptable in short to moderate seas, but tends to underpredict the response in extreme sea states with long wave periods (Matsui, 1986). According to Faltinsen (1998), the wave force autocorrelation spectrum for an angular frequency difference μ may then be approximated by:

$$S_F^{LF}(\mu) = 8\int_0^\infty S_{\zeta\zeta}(\omega)S_{\zeta\zeta}(\omega+\mu)\cdot\left[C_i^{WD}(\omega+\frac{\mu}{2},\beta)\right]]^2 d\omega \qquad i=1,2,6 \quad (2.8)$$

Some coupling effects between WF and LF response was discussed in connection with coupled and uncoupled analysis. For instance, the LF vessel responses are sensitive to the line drag, which are dominated by WF velocities. WF line dynamics, on the other hand, depends on the instantaneous position of the vessel, and thus the magnitude of LF motions.

Low and Langley (2007) noted that, since stochastic linearised damping is based on minimising the mean-squared error across the entire spectrum, the dominance of WF velocities means that the linearisation is likely to be accurate for WF drag, but not necessarily for the LF drag. They also noted that when geometric non-linearity is negligable, the WF line dynamics are no longer seriously influenced by LF vessel motions. They later discovered (Low and Langley, 2008*a*) that when geometric non-linearities are important, such as in shallow water, these linearisation methods gave significantly less accurate results.

2.4.2 LF tension

LF tension can, due to low velocities, normally be modeled by the quasi-static solution. This means that there is little or no dynamic effects on the stiffness, and that the tension can be found by only considering the quasi-static stiffness in Figure 2.10. This is done from the mooring line characteristics, which is a pre-calculated diagram relating quasi-static tension as a function of horizontal distance from the anchor to the top end of the line (Figure 2.7). Since LF motion is sensitive to damping, the LF component of the line tension will be largely influenced by damping as well.

2.5 Combined WF and LF tension

In TD simulations, the coupling between WF and LF response is preserved by solving the dynamic equilibrium equation stepwise. There is hence no need to split the contributions and apply different schemed to each contribution. Frequency domain methods, however, usually can not fully account for the coupling between WF and LF response, and calculates instead the response

statistics separately. Some programs use a simplified coupling between WF and LF response when estimating extreme offset. Just adding the LF extreme and the WF extreme would be very conservative (Kaasen et al., 2007). SIMO offer options for both separation of motion calculations and for simultaneous calculation.

2.6 Mooring line forces

The resulting restoring forces applied to the vessel is a combination of the weight of the mooring lines, and their stiffness properties. The mooring lines need to withstand the forces that arise from the vessels motions and from environmental forces acting on the lines. In addition, as a significant part of the anchor line lies on the sea bed, there will be some friction forces between the sea bed and the mooring lines as well. Figure 2.5 shows the horizontal projection of a typical catenary mooring line cable, and some of the symbols typically included in catenary equations calculation.

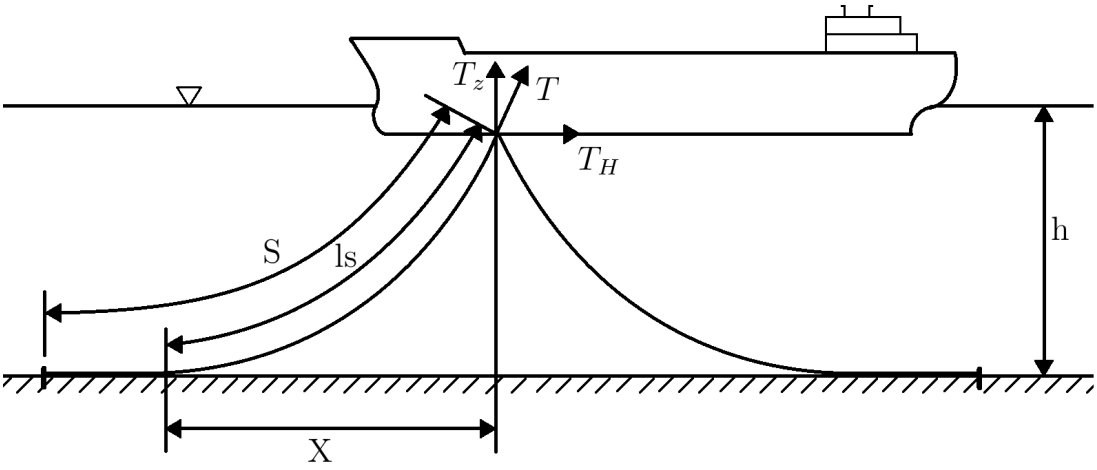

Figure 2.5: Mooring line cable line with symbols

2.6.1 Static configuration

The first step of a mooring analysis is to establish the initial geometry and forces. These are calculated without the impact of environmental loads, and for a two dimensional cable without bending stiffness, the static forces and geometry is defined by Figure 2.6. By neglecting the bending stiffness, current and dynamic effects, the solution can be found analytically from the catenary equations as described in Faltinsen (1998). For a more general approach, Finite Element (FEM) formulations as described by Leonard (1987) can be used.

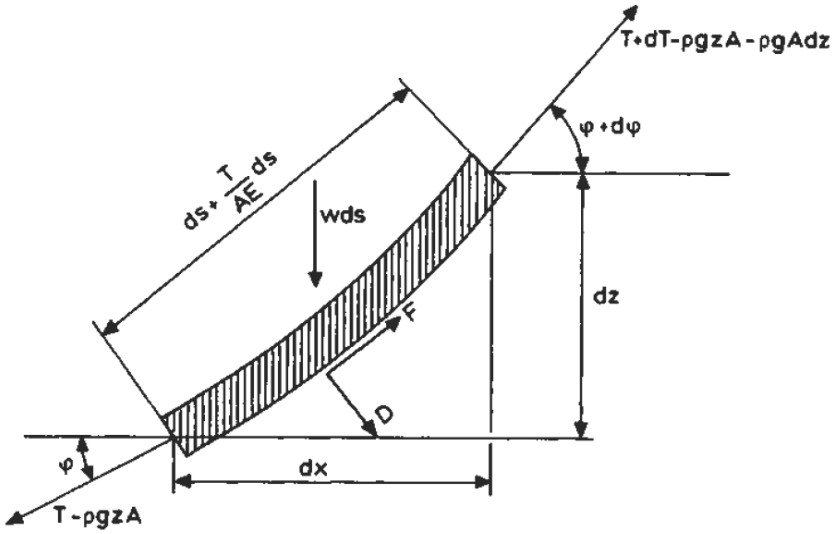

Figure 2.6: Forces acting on an element of a cable (Faltinsen, 1998)

T	-	Axial cable tension (N)
AE	-	Axial elastic stiffness (N)
w	-	Submerged weight per unit length of cable (N/m)
s	-	Arc length (m)
x,z	-	Horizontal and vertical coordinates, respectively (m)
F	-	Tangential hydrodynamic forces (N)
D	-	Transverse hydrodynamic forces (N)
φ	=	Angle between horizontal plane and cable tangent (rad)

The catenary equations may be used to find the static geometry and forces in a mooring line under the following assumptions:

- Constant properties along line
- 2D condition, i.e. no out of plane motion
- Elastic behaviour
- No influence from current

Friction between the cable and sea bed is not included in the catenary equations, but can be included in the solution afterwards. The equations also allow for both inelastic and elastic behavior of the cable lines, and a solution generally requires an iterative process (Garza-Rios et al., 1997).

The catenary equations can be modified to include current, but only in an approximate manner, using a constant mean force applied to an instantaneous geometry. A more generic load case, with for instance depth dependent current, can be included through linearisation, FEM formulation or numerical iteration procedures, as described in Leonard (1987).

2.6.2 Mooring line characteristics

As the top end moves due to the environmental loads, the tension in the cable changes with the line geometry. In addition, the elastic stiffness will increase due to axial elongation. This means that the total stiffness will be a combination of the elastic and the geometric stiffness.

The geometric stiffness is a non-linear quantity, and as a change in offset leads to a larger change in line geometry for slack lines than for tights lines, this stiffness will be most prominent at small offsets. In addition, the touch down point will vary as the line responds to vessel motion and external forces. The variation in touch down point will affect the length of the freely hanging part of the line, and ultimately the geometric stiffness.

The elastic stiffness in steel is linear and increases with an increasing offset. This is the dominating stiffness at large offsets, since a change in offset causes only a small change in geometry for a line that is already tight.

The combination of these two stiffness contributions are clearly shown in Figure 2.7, where the stiffness is the first derivative of the curve.

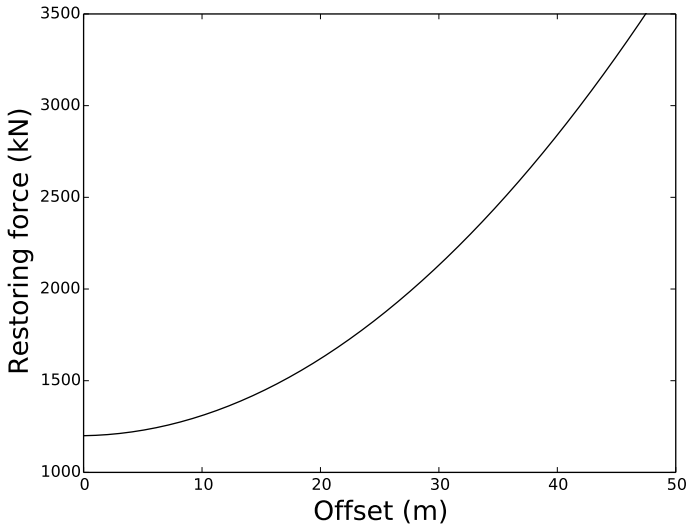

Figure 2.7: Typical line characteristics diagram

2.6.3 Static Equilibrium

Static equilibrium is found when the sum of the horizontal tension in all the lines are balanced by the mean environmental forces (Eq. 2.9). Each line will experience a different tension, based on the pretension and the line's distance to its anchor. At the initial static position, the total tension will consist only of the pretension on the line.

The restoring force is the total horizontal force exerted by the mooring lines, due to a horizontal offset. An example of such a restoring force as a function of offset is shown in Figure 2.8. Offset is here defined as the displacement from the initial static equilibrium position, for which the restoring force will be equal to zero.

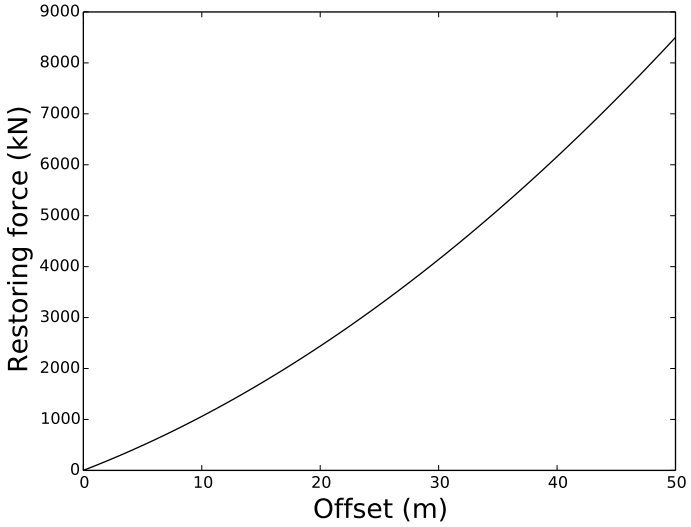

Figure 2.8: Typical restoring force diagram

$$\mathbf{F}^s_{mo}(\mathbf{x}) + \mathbf{F}^s_{wa}(\mathbf{x}) + \mathbf{F}^s_{wi}(\mathbf{x}) + \mathbf{F}_{cu}(\mathbf{x}) = 0 \tag{2.9}$$

$\mathbf{F}^s_{mo}$ - Mooring system force vector (including thruster forces)
$\mathbf{F}^s_{wa}$ - Mean wave-drift forces vector
$\mathbf{F}^s_{wi}$ - Wind force vector due to mean wind speed
$\mathbf{F}_{cu}$ - Current force vector from current acting on vessel

Current forces on the mooring lines may be implemented implicitly through $\mathbf{F}^s_{mo}$ if FEM formulation is used.

The mean wave-drift force in Eq. (2.9) may according to Faltinsen (1998) be expressed as:

$$F^{s,i}_{wa} = 2\int_0^\infty S_{\zeta\zeta}(\omega)\cdot C_i^{WD}(w,\beta)d\omega \quad i = 1,2,6 \tag{2.10}$$

where $S_{\zeta\zeta}(\omega)$ is the wave frequency spectrum, ω is the wave frequency and C_i^{WD} is the wave-drift coefficient defined as

$$C_i^{WD} = \frac{F_i^{WD}(\omega,\beta)}{\zeta_a^2} \tag{2.11}$$

Here F_i^{WD} is the wave frequency and heading dependent drift force, and ζ_a is the wave amplitude.

2.6.4 Effect of Current on Static Offset

As mentioned in Section 2.2.1, the stiffness forces due to mooring and risers will normally not include the effect of current on these elements. The result of calculating the stiffness force in the most loaded line, and the restoring force with and without the effect of current is illustrated in Figure 2.9.

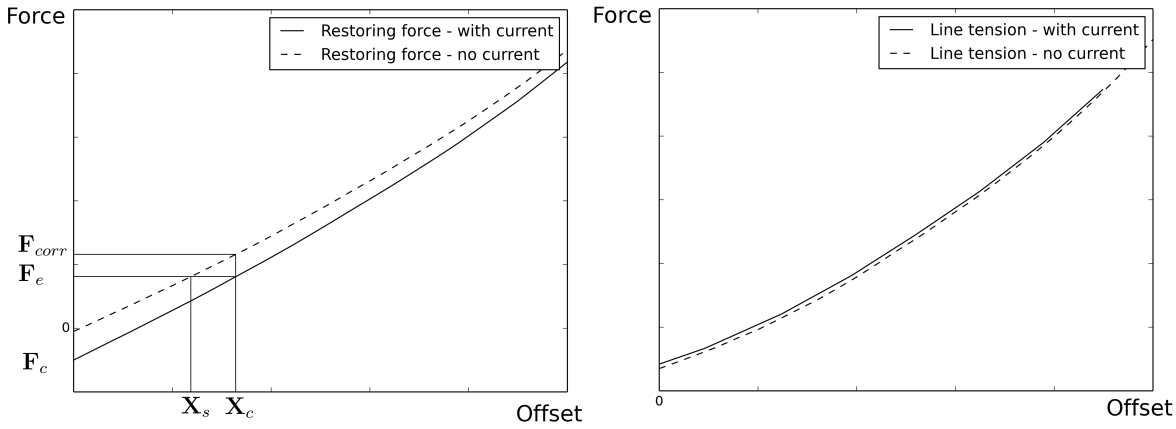

Figure 2.9: Total horizontal restoring force from moorings and risers (left) and line tension in most loaded line (right) given as function of offset (adapted from Ormberg and Larsen, 2004)

where $\mathbf{F_e}$ denotes the mean environmental force, $\mathbf{F_c}$ the current force, and $\mathbf{F_{corr}}$ the environmental force needed to bring the system to the correct mean offset.

From Figure 2.9 two main observations may be made:

1. If the current force on moorings and risers are neglected, the mean offset will be incorrect. Horizontal turret force however, will be correct.

2. If the current force is included as an additional force applied to the vessel, then the mean offset will be correct, whereas the horizontal turret force will be incorrect.

For most cases the line characteristics calculated with and without current will almost coincide, as shown in Figure 2.9. However, this will not necessarily lead to coinciding restoring force characteristics. The reason is that the current will alter the top end angle, and not the line tension.

2.6.5 Dynamic Line Forces

As noted by van den Boom (1985) and Kaasen et al. (2007), the line tension depends not only on the amplitude of the top end excitation, but also on the frequency. At low frequencies, drag forces are negligible and the line geometry is given time to comply to the excitation. The tension can then be found from the quasi-static solution. At higher frequencies the transverse drag may be considerable and act as a drag resistance, restraining the flexibility of the line (Lone, 2009). This in turn, causes a larger part of the motion to be taken by the elastic elongation of the mooring line. The frequency dependence may be expressed as a dynamic motion-to-tension transfer function, as shown in Figure 2.10, where X_d denotes the upper end motion, and T the axial line tension.

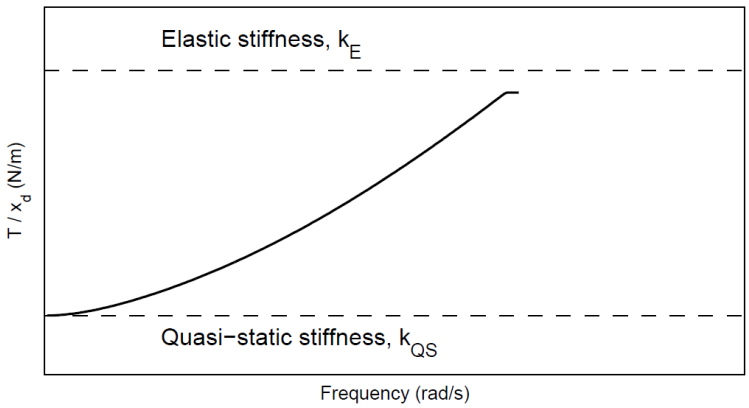

Figure 2.10: Example of motion-to-tension transfer function, with asymptotic values for high and low frequencies (Lone, 2009)

The excitation frequency, and particularly in combination with pretension level, may have a large influence on the line damping as well. At low levels of pretension, damping increases with the frequency of excitation. At higher pretensions however, the damping decreases with excitation frequency. This is because the impedance of stretch, i.e. resistance to change in length, is lower than the transverse impedance, when the pretension is relatively low. For large pretension the opposite is true (Webster, 1994). This can be explained by that pretension alters the hang-off angle, causing horizontal and vertical properties to change in different ways. The resulting property depends on a balance between the relative impedance of these two directions.

2.7 Extreme Response Statistics

To ensure safe operations, it is important to know the maximum offset and line tension a mooring system will encounter during its life time. Since this can not be known in advance, one must rely on a statistical assessment. This section presents a method for assessing the extreme offsets and line tension.

2.7.1 Exact Extreme Value Distribution

Consider a time interval containing N global maxima $\{X_m^{(1)}, X_m^{(2)}, \cdots, X_m^{(N)}\}$, where X_e is the largest of these maxima:

$$X_e = max\{X_m^{(1)}, X_m^{(2)}, \cdots, X_m^{(N)}\} \tag{2.12}$$

The exact extreme value distribution is then given by (Sødahl, 1991):

$$F_{X_e}(x) = P\left[X_e < x\right] = P\left[(X_m^{(1)} < x) \cap (X_m^{(2)} < x) \cap \cdots \cap (X_m^{(N)} < x)\right] \tag{2.13}$$

where N is the number of global maxima. With the assumption that all maxima are identically distributed and statistically independent, the expression may be simplified to:

$$F_{X_e}(x) = P\left[(X_m < x)\right]^N = \left[F_{X_m}(x)\right]^N \tag{2.14}$$

where $F_{X_m}(x)$ is the cumulative distribution of each individual global maxima, and $F_{X_e}(x)$ is the exact cumulative distribution function for the largest maximum, given the mentioned assumptions. Both F_{X_m} and N may in practice be difficult to determine, so instead an asymptotic extreme value distribution is normally used.

2.7.2 Asymptotic Extreme Value Distribution

The exact extreme value distribution will converge asymptotically to one of three distributions as N approaches infinity, depending on the tail behaviour of the initial distribution. The most commonly used distributions in engineering applications have an exponentially decaying tail, which means the exact extreme value distribution will converge into the Gumbel distribution (Sødahl, 1991):

$$F_{X_e}(x_e) = \exp\left\{-\exp\left[-\alpha\left(x - u\right)\right]\right\} \qquad -\infty < x_e < \infty \tag{2.15}$$

where α and u are the scaling and location parameters, respectively. α and u are closely related to the mean and standard deviation.

2.7.3 Parameter Estimation

The scaling and location parameters in Eq. (2.15) can be estimated in several ways. The most common methods are maximum likelihood estimators (MLE), moment estimators, and regression line estimators.

When discussing different methods of parameters estimation, *bias*, *consistency* and *efficiency* are important terms (Myrhaug, 2005). An estimator is unbiased if the expected value of the estimated parameter is equal to the true parameter, i.e.

$$E[\hat{\theta}] = \theta$$

However, the estimator may often only be asymptotically unbiased, i.e:

$$\lim_{n\to\infty} E[\hat{\theta}] = \theta$$

An estimator is also said to be consistent if:

$$\lim_{n\to\infty} Var[\hat{\theta}] = 0$$

It is desirable to have an estimator that is both unbiased and consistent.

Lastly, an estimator is efficient if all available information about the parameter is utilized.

Maximum likelihood estimators are in an asymptotic sense the best estimators (Haver, 2014). They are the most efficient estimators since they utilize as much information as possible from the sample. However, this is just in an asymptotic sense, and for a small or moderate sample, moment estimators may be equally good. Moment estimators will generally not be unbiased, and corrections, e.g. through Monte-Carlo simulations, should therefore be performed. However, whether the estimators are unbiased or not makes little difference if the proposed probabilistic model is poor.

In addition to the above discussion, it is the expected extreme value, located approximately at the 57%-quantile of the Gumbel distribution, that is often of interest (Lone, 2009). Moment estimators are also easier to establish, and their statistical uncertainty can be evaluated by a methods known as the *methods*

of standard errors. The moment estimators are therefore the preferred choice (Sødahl, 1991; Haver, 2014).

The moment based estimators for location and scale parameters of a Gumbel distribution Eq. (2.15) are expressed as:

$$\hat{\alpha} = \frac{1}{S_{X_e}} \frac{\pi}{\sqrt{6}} \tag{2.16}$$

$$\hat{u} = \mu_{X_e} - S_{X_e} \frac{\sqrt{6}}{\pi}\ 0.57722 \tag{2.17}$$

where μ_{X_e} and S_{X_e} are the mean and standard deviation of the extreme value sample, respectively.

Estimating a distribution from a sample will contribute to the statistical uncertainty. This uncertainty will decrease with increasing sample size, and for a given sample size the uncertainty will increase with the number of sample moments needed to estimate the distribution, which is two in the case of a Gumbel distribution.

2.7.4 Probability Paper

In order to assess whether the proposed probability model is reasonable the observations are plotted on a properly created probability paper. If the proposed model is correct then the observations should fall on a straight line. This is a subjective method, as it relies on a visual and subjective way of judging whether deviations from the straight line is within acceptable limits. For an ordered extreme value sample

$$\{x_1, x_2, x_3, \cdots, x_k, \cdots, x_n\}$$

one can estimate the cumulative distribution function as follows (Myrhaug, 2005).

$$\hat{F}_X(x_k) = \frac{k}{n+1} \tag{2.18}$$

where k is the number of observations less or equal to x_k, and n is the total number of observations.

Eq. (2.15) is transformed into a linear equation, and the axes of the probability paper are given by:

$$\begin{aligned} \text{Vertical axis:} \quad & Y = \text{-ln(-ln}(F_{x_e})) \\ \text{Horizontal axis:} \quad & X \end{aligned} \tag{2.19}$$

where Y is the linearised function value. The sample may now be plotted in the coordinate system created by Eq. (2.19), by generating as many evenly spaced function values between 0 an 1, as the number of sample points. These should be converted into linearised function values, Y, and plotted against the sample values.

To quantify the uncertainty in the estimated extreme value distribution, Monte Carlo simulation may be performed. It has the advantage that the result will always converge to the correct answer if the number of data points in a sample becomes sufficiently large (Haver, 2014). By running a multitude of Monte-Carlo simulations one can establish a confidence interval which will give a range of values the distribution is likely to fall within, with a certain probability. The procedure for running such analyses is described by Leira (2010).

2.7.5 Long Term Extremes

The method above is used to predict the short term extremes, i.e. maximum values during one sea state. For a long term assessment of extremes, a common simplified approach is to utilize an *environmental contour line*, as described by Kleiven and Haver (2004). In the *environmental contour line* approach, the worst short term distribution in terms of response, with a certain annual probability of exeedance, is used as a long term distribution. This is done by going to an artificially high level of the exeedance on the distribution, often the 90 %-quantile, to account for short term variability. For comparison, the expected value in a Gumbel distribution is roughly located at the 57 %-quantile, while the most probable maximum (MPM) is roughly located at the 37 %-quantile. In the case study, an environmental contour line with an annual probability of exeedance of 10^{-2} (corresponding to a 100year wave) is used. Extreme samples from short term simulations are established, an a rough estimate of the short term extremes are discussed.

Chapter 3
Damping

Several damping mechanisms are present in a moored floating system. Since LF motion is a resonance motion, a good estimate of the damping level is important. This is often one of the major shortcomings of approximate methods. Which damping contributions are important, largely depends on the system, environmental conditions and type of motion. Here, only the most important damping contributions for horizontal motion, i.e. surge, sway and yaw are discussed, as well as viscous roll damping. A more thorough description of various damping components present in a moored system is presented by Nilsen (2007).

The damping contributions acting on a hull may be divided into (Chakrabarti, 2005):

- Radiation damping due to wave making
- Viscous hull damping
- Wave drift damping
- Mooring line damping

In addition to these, structural damping, damping from wind, and damping introduced by the numerical procedures may be present. However, these contributions are small compared to the list above.

Radiation damping arises from wave making, and is determined from first order potential theory. This damping force is linearly proportional to the wave amplitude, and is seen to exhibit a strong dependence on wave frequency and the degree of submergence (Næss and Moan, 2013). It is an important damping contribution on WF motions, but negligible for LF motions as these slow motions have an insignificant contribution to wave making.

3.1 Viscous Hull Damping

Viscous effects may be divided into skin friction and viscous forces due to the pressure distribution around the hull (Faltinsen, 1998). The latter effect is often associated with generation of vortices, or eddies, and is hence usually referred to as eddy-making damping. Eddy-making damping are important contributions in sway and yaw, and can in some cases be calculated by strip theory and the cross-flow principle.

In roll, viscous damping is is mainly due to bilge keels, eddy-making resistance of the hull, and hull friction. Among these, bilge keels are normally the biggest contributor.

In surge, skin friction will be the largest contributor to viscous hull damping.

The effect of skin friction and effects due to pressure distribution is often collectively referred to as drag.

3.2 Wave Drift Damping

In the horizontal plane, wave-drift damping may also be an important contribution for hull damping. For higher sea states this may also be the dominant hull damping component (Faltinsen, 1998)

Wave drift damping is caused by the waves and can be seen by comparing free-decay model tests of a ship in still water and in regular waves. One will then observe that the oscillation decays faster in the presence of waves, meaning an extra damping occurs. Wave drift damping is often the most important hull damping contribution of LF motions. It is proportional to the square of the incoming wave amplitude and proportional to the slowly varying velocity of the body. Wave drift damping is due to change in the mean second order force (mean drift) upon a body when it moves with a constant speed against, or in the direction of incoming harmonic waves, and is given by (Grue, 1996):

$$2U \int_0^\infty \frac{\partial T}{\partial U} S(\omega) d\omega \tag{3.1}$$

where U denotes LF velocity of the body and T the mean second order force in regular waves divided by the amplitude squared. $\frac{\partial T}{\partial U}$ is evaluated at $U = 0$.

Wave drift damping has both a mean and a time dependent part. However, as Wichers and van Sluijs (1982) showed, time-dependent wave drift damping may

be replaced by a constant wave damping coefficient or neglected.

3.3 Yaw Damping

The current yaw moment can in many cases be evaluated by use of the cross-flow principles and strip theory. This can be done under the following assumptions (Faltinsen, 1998):

- Flow separates due to cross-flow past the ship.
- The longitudinal and the transverse current components do not influence one another.
- The transverse force is mainly caused by flow separation.

The yaw moment due to current flow is the sum of the Munk moment obtained from potential theory, and the viscous yaw moment due to cross-flow. The viscous cross-flow moment can itself be divided into two contributions; current drag from a purely translation motion, and a contribution due to pure yaw velocity, as indicated by figure 3.1. The former is obtained from quadratic current force coefficients and the instantaneous magnitude of the translational relative velocity between the vessel and the fluid. The Munk moment is normally included in the quadratic current force coefficients, which gives a relationship between current velocity and the current force exerted on the vessel. It is therefore excluded from the equations of motions (Eq. 4.1).

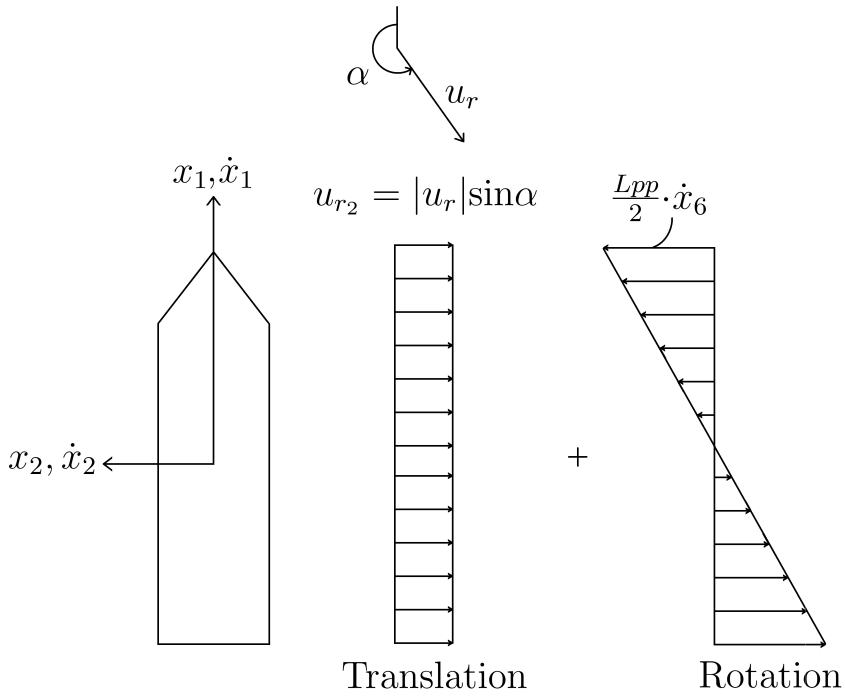

Figure 3.1: Separation of cross-flow due to translation and rotation (SIMO project team, 2012)

3.4 Mooring Line Damping

The presence of mooring lines will introduce additional damping on the system, which in deep water or in areas with large currents may constitute a significant contribution to the total damping. Larger depth will increase the mooring line damping, both because vessel motions are larger, and because of larger suspended lengths.

The main damping contributions from mooring lines are due to drag. The relative velocity formulation of the drag will produce both an excitation and a damping force (Næss and Moan, 2013). Drag forces are proportional to the relative velocity of the water particle and the mooring line squared, and the drag term on a unit length of the line due to a horizontal motion may be expressed by the drag term of Morison's equation:

$$F_d = \frac{\rho}{2} C_d D |V_{rel}| V_{rel} \tag{3.2}$$

where C_d is the drag coefficient, D the line diameter, V_{rel} the relative horizontal velocity between current and line segment, $V_{rel} = U_c - \dot{r}$. Here, U_c and $\dot{r}$ are the horizontal velocity of current and line element, respectively. By expanding the

relative velocity term, Eq. (3.2) gives:

$$\begin{aligned} F_d &= \frac{\rho}{2} C_d D (U_c - \dot{r})^2 \\ &= \frac{\rho}{2} C_d D (U_c^2 - 2U_c\dot{r} + \dot{r}^2) \end{aligned}$$

where the coupling term $-2Ur$ introduces a damping force acting against the motion direction.

Mooring lines will also introduce some structural damping and damping due to bottom friction. The former contribution is usually very small, and may therefore be neglected. This is particularly true for steel catenary systems, as there is virtually no energy dissipation in the cyclic motion (Magnussen, 2013). Damping from bottom friction may provide a notable contribution to the total damping, but due to reasons described in the results chapter (Chapter 7), bottom friction is not included in the models.

Chapter 4
Programs

4.1 SIMO

SIMO is a computer program for simulation of motion and station-keeping behaviour of floating vessels and suspended loads. It features non-linear time domain simulation for wave-frequency forces, as well as for low-frequency forces. It offers an accurate description of vessel response. However, modelling of mooring line forces, as well as the interaction between vessel and mooring lines, are only available in a simplified manner for large volume structures.

4.1.1 Vessel motion

SIMO solves the dynamic equation (4.1) in time domain through step-by-step numerical integration.

$$\mathbf{M}\ddot{\mathbf{x}} + \mathbf{C}\dot{\mathbf{x}} + \mathbf{D}_1\dot{\mathbf{x}} + \mathbf{D}_2\mathbf{f}(\dot{\mathbf{x}}) + \mathbf{K}(\mathbf{x})\mathbf{x} = \mathbf{q}(t, \mathbf{x}, \dot{\mathbf{x}}) \tag{4.1}$$

where

$\mathbf{M}$	-	Frequency dependent mass matrix
$\mathbf{C}$	-	Frequency dependent potential damping mattrix
$\mathbf{D}_1$, $\mathbf{D}_2$	-	Linear and quadratic damping matrix, respectively
$\mathbf{f}$	-	Vector function where each element is given by $f_i = \dot{x_i}\|\dot{x_i}\|$
$\mathbf{K}$	-	Hydrostatic stiffness matrix
$\mathbf{x}$, $\dot{\mathbf{x}}$, $\ddot{\mathbf{x}}$	-	Position, velocity, and acceleration vector
$\mathbf{q}$	-	Excitation force vector

$\mathbf{q}(t, \mathbf{x}, \dot{\mathbf{x}})$ consist of wind drag, 1st order wave, 2nd order wave, current, and other forces such as wave drift damping, specified forces and mooring.

SIMO differentiates between large volume and small volume structures. For large volume structures, such as tankers and FPUs, the dynamic equilibrium can be

solved either by a convolution integral, or by separation of motion. In the latter method, WF response is solved in FD with constant stiffness matrix and zero quadratic damping. In the former approach, the added mass and damping is Fourier transformed to give the retardation functions:

$$\mathbf{h}(\tau) = \frac{1}{\pi}\int_0^\infty \mathbf{c}(\omega)\cos(\omega\tau) - \omega\mathbf{a}(\omega)\sin(\omega\tau)d\omega \tag{4.2}$$

where $\mathbf{c}(\omega)$ and $\mathbf{a}(\omega)$ are the frequency dependent damping and added mass, respectively. The total motion is simulated in time domain.

In order to preserve the coupling effects between WF and LF responses, in addition to any memory effects from the response history, the solution by convolution integral is chosen for the case study.

In SIMO, viscous sway force and yaw moment on the hull are calculated from quadratic current coefficients. These coefficients normally also include the munk moment. Hydrodynamic coefficients are precalculated by diffraction/radiation solvers such as WAMIT or WADAM.

4.1.2 Line Tension

Calculation of mooring line tension for body type 1 (see Table 4.1) in SIMO is only available by means of a quasi-static solution. This ignores any dynamic effects, such as excitation frequency, the effect of current on the stiffness characteristics, change of touchdown point, etc. Body type 1 is used throughout the case studies

Three types of methods may be chosen: shooting method, shooting method with simplified dynamics, and FEM. The shooting methods are based on the catenary equations, where simplified dynamics accounts for the effect of drag loading on the line in a simplified manner. Simplified dynamics is however, not available for large volume structures (body types 1 and 2). With a finite element formulation, each element is assumed to form a catenary. The mooring line is assumed to be 2D in a local coordinate system, i.e. transverse bottom friction and out-of-plane bending is not included.

For a quasi-static analysis the effect of transverse drag forces on the lines are neglected. The line forces are thereby only determined by the position of the two end nodes. The tension is found by interpolation on the line characteristics table, which has been precalculated. Dynamic effects may cause line tension to be different than the one predicted by quasi-static analysis. This is important to

Table 4.1: Large volume body types for simulations in SIMO

Body type	Description
1	Total motion is simulated in time domain. 6 DOF. WF motion is calculated from *wave elevation-to-force* transfer functions.
2	Frequency domain WF motion (pre-calculated), time domain LF motion. 6 DOF. WF motion calculated from *wave elevation-to motion* transfer functions.

notice, as only the quasi-static solution is available for body type 1.

4.2 RIFLEX

RIFLEX is a non-linear finite element (FEM) program for calculating tensions and displacements in slender structures.

4.2.1 Vessel motion

WF vessel motion can either be applied by first order elevation-to-motion transfer functions, or from predescribed file. LF motion may be applied through direct input of complex response spectra, or from predescribed file as well. SIMO output files containing vessel position may be used as such predescription files, and is the alternative for including the coupling between WF and LF motion. This approach is used in the case study to preserve this type of coupling (type 2). By specifying the vessel motion from predescription files one have the opportunity to focus on a specific line, without modelling the whole mooring system. This may drastically reduce the computation time.

4.2.2 Line Tension

RIFLEX solves the dynamic equilibrium equation (4.3) numerically in time domain:

$$\mathbf{R}^I(\mathbf{r}, \ddot{\mathbf{r}}, t) + \mathbf{R}^D(\mathbf{r}, \dot{\mathbf{r}}, t) + \mathbf{R}^S(\mathbf{r}, t) + \mathbf{R}^E(\mathbf{r}, \dot{\mathbf{r}}, t) \tag{4.3}$$

where

- $\mathbf{R}^I$ - Inertia force force
- $\mathbf{R}^D$ - Damping force vector
- $\mathbf{R}^S$ - Internal structural reaction force vector
- $\mathbf{R}^E$ - External force vector
- $\mathbf{r}, \dot{\mathbf{r}}, \ddot{\mathbf{r}}$ - structural displacement, velocity and acceleration, respectively

Equation (4.3) can be solved in a fully non-linear or in a linearised analysis. The former accounts for all non-linear effects discussed in previous chapters, while the latter requires a linearisation of the left hand side of the equation. In the linearised method, the non-linear hydrodynamics are still accounted for, making it appealing for e.g. deep water problems or where quadratic line drag is important, but where non-linearities in e.g. geometric stiffness is less prominent.

In a static analysis, an initial configuration is found by an equilibrium iteration until the external force is balanced by the internal structural reaction force. The initial configuration must be established before a dynamic simulation can be performed. For each time step in the dynamic analysis, the external loading should be balanced by inertia, damping and structural forces.

Mooring lines are modelled as bar elements or beam elements, and complex cross sections, as well as material and hydrodynamic properties are possible. Line drag, and hence the line damping, is included through the external force vector by a generalized Morison formulation. This assumes that the option for wave forces on the lines are activated. Prescribed vessel motions are also included in the external force vector.

RIFLEX may account for several non-linear effects, such as:

- Geometric stiffness
- Non-linear material properties
- Non-linearities due to generalized Morison formulation
- Integration of loading at actual surface elevation
- Contact problems

where geometric stiffness and contact problems are the most important ones for mooring systems at shallow and moderate water depth. Bottom friction forces are not automatically taken into account when calculating the line characteristics. Non-linearities due to generalized Morison becomes increasingly important as water depth increases.

4.3 SIMA

SIMA provides a graphical interface and communication between SIMO and RIFLEX, allowing the coupled response to be calculated for each time step, through equilibrium iterations. The force model of the floater from SIMO is then

implemented as nodal forces at the top end of the FE model of the mooring lines and risers from RIFLEX. A dynamic equilibrium is found through an iteration procedure, taking both vessel and structural response into account. This way, the LF damping and current forces from mooring lines are included automatically in an accurate manner.

Chapter 5
Case Study

The purpose of the case study is to investigate the vessel offset and line tension in the most loaded line for coupled and uncoupled analysis, as well as the relationship between environment, damping estimate and system response. This is performed by an approach similar to one described by Ormberg et al. (1998). The procedure is also presented schematically in a flow chart in Appendix B.

The analyses are performed by the computer programs SIMO, RIFLEX and SIMA, the latter being an interface which enables a coupled interaction between the former two. The uncoupled analysis is performed by using a linear damping coefficient, estimated in the coupled analysis, as input. The results are presented and discussed in chapter 7.

5.1 System Description

The system is a turret-moored FPSO located in the Åsgard field at 320 meters water depth. The vessel main particulars and dominant eigenperiods are summarized in tables 5.1 and 5.2

Table 5.1: Main particulars

Length over all (m)	278
Length in waterline (m)	250
Width (m)	42.5
Draft (m)	15.97
Displacement (tonnes)	148.200

Table 5.2: Eigenperiods (calculated by SIMO)

DOF	Surge	Sway	Heave	Roll	Pitch	Yaw
Period (s)	257.39	188.41	11.22	19.46	9.94	1936.34

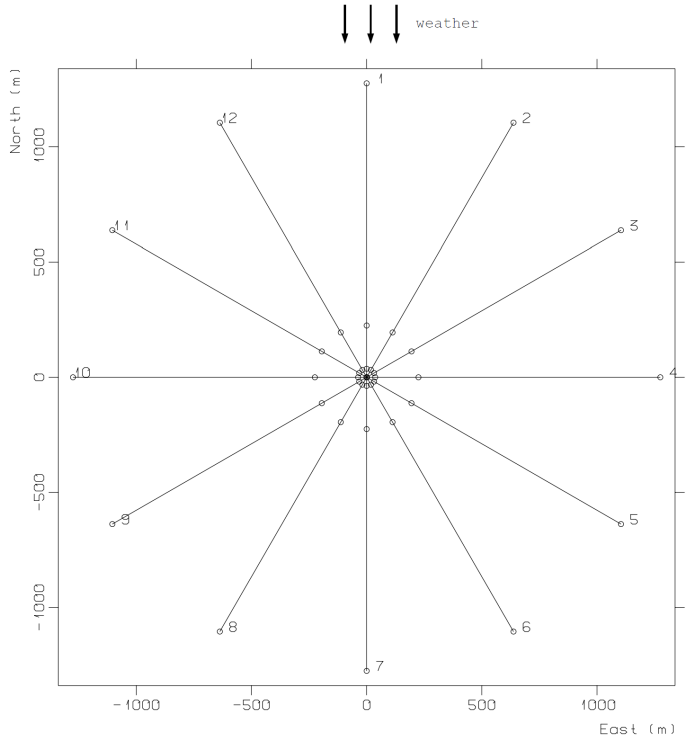

Figure 5.1: Overview of the case study mooring system

The FPSO is fitted with an internal turret, and is held in place by twelve evenly distributed steel catenary mooring lines (see Figure 5.1). The fairlead positions are located 48.32 meters ahead of the vessel's center of gravity, located 11.72 meters aft of the midship, and 15.97 meters below the water line. The main particulars of the mooring system are shown in Table 5.3.

Table 5.3: Main particulars of mooring system

Distance from COG to turret center (m)	48.32
Vertical distance from waterline to fairlead (m)	15.97
Number of lines	12
Pretension (all lines) (kN)	1200
Turret diameter (m)	8.85

The twelve mooring lines are numbered clockwise with line 1 pointing north, and each line is divided into four segments. Their properties are shown in Table 5.4, where segment 1 is connected to the anchor, and segment 4 is attached to the turret. No clump weights or buoyancy elements are attached to the lines.

Table 5.4: Characteristics for each line segment

Segment number[a]	Type of line	Diameter (mm)	Length (m)	Wet weight (kN/m)
1	Chain (R4)	114	930	2.2390
2	Chain (R4)	147	285	3.7230
3	Wire	121	300	0.5873
4	Chain (R4)	114	50	2.2390

[a]Numbered from anchor

An extra heavy chain is used near the seafloor (segment 2) to provide sufficient weight and stiffness.

5.2 Environmental Conditions

All environmental data are taken from *Åsgard Metocean Design Basis* (Nygaard and Eik, 2004), where the peak of the 100-year contour line is chosen as the base case wave condition. The methodology for establishing such a contour line is described by Haver and Winterstein (2008) and by Kleiven and Haver (2004). A summary of the environmental conditions for all the case studies is given in Table 5.5.

The water surface is modelled by a double peaked spectrum, known as the Torsethaugen spectrum, which is a model for wind driven waves and swell in combination. The spectrum is given by the significant wave height (H_S) and peak period (T_P) only, which are taken from the Table 5.5. Wind is modelled by a ISO 19901-1 (NPD) spectrum. The current has a linear profile, which in the base case decreases from 0.9 m/s at the surface to 0.0 m/s at the sea floor. All environmental forces are applied directly at the bow, i.e. the vessel experiences head sea conditions.

5.3 Cases

The case study is divided into several parts, in order to study different effects. These may be summarized as:

- Base case with extreme 100 year storm conditions

- Alternative current profile
- Alternative Hs and Tp
- Alternative heading
- Damping sensitivity study with damping fractions 0.1, 0.5 and 2.0 of the base case

where base case denotes the system and environmental condition as described above.

In order to study the effect of current on the mooring line damping, an alternative current profile is investigated. This alternative case is identical to the base case, apart from having a current profile which decreases linearly down to 0.5 m/s at the seabed instead of 0.0 m/s.

An alternative Hs and Tp combination is investigated in order to study the coupling between the mooring line damping, and the WF and LF motion. All other parameters are identical to the base case.

An alternative heading of 15 degrees is imposed in order to investigate the effect on the damping estimate on the uncoupled results. The environmental conditions are identical to those in the base case.

Lastly, a damping sensitivity study is performed, in order to investigate the effect of the uncertainty in the damping estimate on the system responses. The environmental conditions are the same as for base case, but the fractions of the damping estimate obtained in the coupled base case are varied. Fractions investigated are 0.1, 0.5 and 2.0 of the damping estimate for a single seed in the base case.

Table 5.5: Summary of environmental conditions

	Head (deg)	Hs (m)	Tp (s)	U^{wi} (m/s)	U_s^c (m/s)	U_b^c (m/s)
Base Case	0	16.0	18.1	0.32	0.9	0.0
Altt current profile	0	16.0	18.1	0.32	0.9	0.5
Alt. Hs and Tp	0	12.0	12.5	0.32	0.9	0.0
Alt. heading	15	16.0	18.1	0.32	0.9	0.0

where U^{wi} is the average wind speed, and U_{sf}^c and U_{sb}^c is the current velocity at the surface and the seabed, respectively.

Chapter 6
Modelling

Several modelling considerations must be made, due to restrictions in the software, stability of the results and numerical procedures, to obtain similarities between models, and due to the purpose of the thesis. These considerations, a description of the models, as well as the procedure for estimating the mooring line damping, are outlined in this chapter.

6.1 Model Damping

6.1.1 Estimation of LF Surge Damping from Mooring Lines

The main scope of the thesis involves comparing results from coupled and uncoupled analysis using damping estimates from the coupled analysis. This section provides a description of the methodology for obtaining a linear LF damping estimation, due to mooring lines and risers. The procedure requires simultaneous time series of vessel position and total horizontal LF force from mooring lines and riser. The procedure is taken from Ormberg et al. (1998), and a summary may be seen in the flow chart in Appendix B.

The main assumption of the estimation technique is that the horizontal force can be approximated as:

$$F_m = m\ddot{x} + c\dot{x} + k_1 x + k_2 x^2 \tag{6.1}$$

where

F_m	-	Total horizontal LF dynamic force from mooring lines and risers
	-	(i.e. force relative to static equilibrium)
x	-	Dynamic LF vessel displacement relative to static equilibrium
$\dot{x}, \ddot{x}$	-	LF vessel velocity and acceleration
m	-	Slender structure mass
c	-	Linear damping coefficient
k_1, k_2	-	Linear and quadratic stiffness coefficients

The unknown model coefficients (m, c, k_1, k_2) can be estimated from a least square fit in time domain. The mean square error ε expresses the deviation between the proposed model F_m and actual measured force F over a time period T, and is defined as:

$$\varepsilon^2 = E[(F - F_m^2)] = \frac{1}{T}\int_0^T (F - m\ddot{x} - c\dot{x} - k_1 x - k_2 x^2)^2 dt \tag{6.2}$$

As the main purpose is to estimate an equivalent linear damping to be applied in de-decoupled vessel motion analysis, the coefficients are estimated in the following way:

- k_1 and k_2 are estimated from the restoring force characteristics considering mooring lines as well as risers
- A rough estimate of the mass contribution from mooring lines and risers is sufficient, as the slender structure mass is negligible compared to the vessel mass. In most situations it is acceptable to neglect the slender structure mass.

Having established m, k_1 and k_2, the least square damping estimator can be obtained from the requirement $\partial\varepsilon^2/\partial c = 0$, which yields the following relationship:

$$c = \frac{E(\dot{x}F) - mE(\dot{x}\ddot{x}) - k_1 E(x\dot{x}) - k_2 E(x^2\dot{x})}{E(\dot{x}^2)} \tag{6.3}$$

It can be shown that the limiting value of the damping estimator as $T \to \infty$ is given by:

$$c = \frac{E(\dot{x}F)}{E(\dot{x}^2)} \tag{6.4}$$

In practice, F and x are found by low-pass filtering of the zero-mean total signals. Velocity and acceleration are then found by numerical derivation of the low-pass filtered displacement. In order to obtain stable damping estimates one should use full motion cycles of the low-pass filtered displacement time series, i.e. the time window should cover the interval between the first and the last zero up-crossing

of the signal.

An alternative approach, which allows an assessment of the statistical uncertainty related to the estimated damping coefficient can be performed by the following steps:

1. Identify all motion cycles in the low-pass filtered vessel displacement time series.

2. Apply the least square damping estimator for each cycle.

3. Compute an representative damping estimate by averaging over all cycle estimates:
$$\bar{c} = \frac{1}{N}\sum_{n=i}^{N} c_i$$
where c_i is the damping estimate in cycle 'i', and N the total number of identified cycles.

4. The standard deviation of the damping estimate can be expressed as: $\sigma_{\bar{c}} = \sigma_c/\sqrt{N}$ where $\sigma_c^2 = \frac{1}{(N-1)}\sum_{i=1}^{N}(c_i - \bar{c})^2$

The first estimation approach was chosen, which in practice was handled by a post processing code in Python 2.7, shown in Appendix E.

6.1.2 Addition Mooring Line Damping

The mooring line damping estimate obtained in the previous section is applied as a constant linear coefficient in surge. In addition to surge, the linear line damping contribution in sway and yaw, as well as the linear coupling terms between sway and yaw, is estimated from the damping coefficient in surge through the following relationships:

$$\begin{aligned} B_{22} &= B_{11} \\ B_{26} &= -B_{62} = -x_T \cdot B_{22} \\ B_{66} &= x_T^2 \cdot B_{22} \end{aligned} \tag{6.5}$$

where x_T is the distance between the horizontal vessel center of gravity and turret center, and B_{ij} denotes element ij in the linear vessel damping matrix in Eq. (4.1).

6.1.3 Yaw Damping

The SIMO model does not account for the effect from the yaw-induced cross-flow, described in Section 3.3. This must therefore be included as a separate

yaw damping term. When this is included, the yaw moment is given as (SIMO project team, 2012):

$$q(\alpha) = C_6(\alpha)|u|^2 + b_{66}\ \dot{x}_6|\dot{x}_6| \tag{6.6}$$

where

$C_6(\alpha)$	=	Quadratic current coefficient in yaw
α	=	Incident current angle relative to direcetion of LF vessel velocity
u	=	Relative translational velocity between fluid and LF vessel velocity
b_{66}	=	Quadratic damping coefficient in yaw due to a pure yaw velocity
$\dot{x}_6$	=	Yaw velocity

The quadratic damping coefficient b_{66} can be estimated by use of strip theory, and by assuming constant drag properties along the vessel. The forces from the yaw-induced motion may then be shown to be linearly distributed along the vessel as seen in figure 3.1.

In the cross-flow principle the yaw velocity may be expressed by the sway velocity through the relationship:

$$\dot{x}_2 = (x\dot{x}_6)$$

By normalizling the current force coefficient in sway with regards to the vessel length, $C_2' = \dfrac{C_2(90^\circ)}{L_{pp}}$, the force over one strip is then given as:

$$dF = C_2'(x\dot{x}_6)|(x\dot{x}_6)|dx \tag{6.7}$$

The contribution of each strip to the yaw moment is then:

$$dM = C_2'(x\dot{x}_6)|(x\dot{x}_6)|xdx \tag{6.8}$$

By integrating over the length of the vessel one obtain the following relationship:

$$\begin{gathered} M = \int_{-L_{pp}}^{L_{pp}} C_2'(x\dot{x}_6)|(x\dot{x}_6)|xdx = -\frac{L_{pp}^3 \cdot C_2(90^\circ)}{32}\dot{x}_6|\dot{x}_6| = b_{66}\ \dot{x}_6|\dot{x}_6| \\ \Downarrow \\ b_{66} = -\frac{L_{pp}^3 \cdot C_2(90^\circ)}{32} \end{gathered} \tag{6.9}$$

b_{66} is included in the quadratic damping matrix, D_2, in Eq. (4.1).

6.1.4 Roll Damping

As viscous effects are important contributions to roll damping, only including the damping obtained from radiation/diffraction analysis will lead to artificially large roll motions. In order to overcome this problem a sufficient damping level is added in terms of a linear coefficient. Only a rough estimate of 10% of critical is used. Since surge is the main motion of interest, and an accurate estimate of roll damping is not necessary.

6.1.5 Simplified Wave Drift Damping

Wave drift forces is included in a simplified manner as:

$$\hat{F}_i(t) = F_i(t)(1 + c_{wd} v_{wr}) \tag{6.10}$$

where v_{wr} is the difference between current and body velocity in the wave direction, $F_i(t)$ is the uncorrected wave drift force and c_{wd} a linear wave drift damping coefficient. c_{wd} is implemented as a function of estimated peak wave period, and is fixed during the simulations.

6.2 Specified Forces

To ensure a correct draught, corresponding to the vessel RAOs, a specified force which compensates for the weight of the mooring system is applied. This specified force is obtained from the initial position and applied as a constant vertical point force acting at the fairlead. This is performed in both the coupled and the uncoupled model.

As mentioned in Section 2.2, the mean current force on the mooring lines needs to be estimated and included in the uncoupled model in an approximate manner. The mean current force is estimated from a coupled analysis so that the vessel assumes the same static offset in the coupled and the uncoupled models, when only exposed to current.

6.3 Simulation Length

It is important to ensure a sufficient number of motion cycles, in order to achieve an acceptable level of uncertainty in the statistics. This is mainly a concern for LF response, as the excitation period is much longer than for WF motion. Ormberg et al. (1998) showed that a simulation time of more than 2 hours is normally

sufficient for capturing the LF behaviour. The simulation length in the case study comprises 3 hours of steady state response. When comparing responses from two different wave spectra the responses can not be compared directly. Instead, a number of simulations must be performed, and the statistical parameters compared. This is relevant, for instance, when comparing results from the case with alternative Hs and Tp with the base case.

In order to reduce the statistical uncertainty related to both extreme estimates and damping estimates, a sufficient number simulations should be performed. In each simulation, the wave elevation realization must be unique in order to contribute into lowering the statistical uncertainty. In many cases at least 30 simulations is desirable. However, the required number depends on the purpose of the analysis (Baarholm, 2014). Uniqueness is ensured by varying the seeds, i.e. the random numbers used to generate the water surface, as described in Section 2.1.2.

6.4 Automatic Thruster Assistance

In order to ensure a weather vaning condition, an automatic thruster assistance (ATA) is needed. ATA is included in a simplified manner as a hydrostatic stiffness term in yaw.

Chapter 7
Results and Discussion

7.1 General Description

This section presents and discusses the results of the cases described in Section 5.3. To summarize, these are:

- Base case with extreme 100 year storm conditions
- Alternative current profile
- Alternative Hs and Tp
- Alternative heading
- Damping sensitivity study with damping fraction 0.1, 0.5 and 2.0 compared to base case

A summary of the environmental conditions is given in Table 5.5.

7.2 Result Considerations

When interpreting the results, several important considerations should be kept in mind. These are discussed before the results are presented.

7.2.1 Definitions and General Comments

In all cases, vessel offset is measured from initial position without environmental forces, and denotes a motion along the global x-axis.

Line tension results are presented for line 1 (windward line), which have been verified to be the most loaded line for all cases except alternative heading. However, offset and line tension is not discussed for alternative heading as the focus

is on the damping estimate.

The linear damping estimates, B_{11}, refers to a local surge motion of the vessel in the uncoupled model. Furthermore, the mooring line damping is non-linear of nature. This non-linearity is fully accounted for in the coupled model.

Mean values denotes the dynamic mean, i.e. the average value of the time series, and not the static offset due to mean environmental forces. Due to various dynamics effects, such non-linear stiffness and drag, these will not necessarily be the same.

The standard deviations refers to the instantaneous values of the time series, with previously mentioned definitions.

Maximum values denotes the maximum observed during a 3 hour sea state.

The coupled and the uncoupled surface realization are generated by the same seed numbers, and verified to be equal. Wind and waves are generated by the same seed numbers.

The current velocity at the surface is used on the whole vessel depth when calculating the current forces on the hull. Depending on the draught, heading and current profile, the current forces may therefore be overestimated.

The mean current forces on the lines are only included in an approximate manner in the uncoupled model. They have been estimated by an iteration procedure until the two models assume the same static offset, when only exposed to current. This means that the mean current forces, strictly speaking, are only valid for these static offsets. Once wind and waves are introduced the vessel will assume a different mean offset, with oscillations around this mean. It is assumed that, due to moderate water depth and small changes in geometry, this mean current force will provide a satisfactory approximation during the case studies.

For extreme response estimates in time domain, the wave elevation should preferably be generated by stochastic amplitudes. However, stochastic amplitudes are not implemented in SIMO for use with Fast Fourier Transform (FFT), and hence deterministic amplitudes are instead used. The implications are discussed in Section 2.1.2.

Some numerical damping and global stiffness damping is added to gain stability in the calculations. They should however, only have a minimal effect on the

results as these damping levels are low.

Wave force on the mooring lines are not included in order to study the effect of current on the mooring lines only, and because SIMO and RIFLEX includes wave forces on the lines differently. Hence, the mooring line geometry only depends on the top end motion, and also the line current for the coupled model.

LF forces are obtained from drift coefficients, and not the full quadratic transfer functions (QTF), a method known as Newman's approximation. The application of Newman's approximation tends to underpredict the response in extreme sea states with long wave periods.

LF motion, and in turn the damping estimate, is generally associated with larger statistical uncertainty than WF motion due to fewer motion cycles. However as Ormberg et al. (1998) showed, the accumulated mean of the damping estimate will converge after a simulation time of 1.5 hour to 2 hours.

The damping contribution from the mooring lines in sway and yaw are estimated from the linear damping coefficient obtained in surge. With head sea conditions, it is assumed that this will provide a sufficient estimate for these degrees of freedom, so that they will not significantly influence the results presented. This assumption is briefly discussed in the results.

The steady-state solution is reduced during the damping sensitivity study, as the transient decay time generally depends on the damping level. This is illustrated in Appendix D. After a visual inspection of the time series the transient time was adjusted from 200s to 3000s, leaving 8000s, or approximately 2,2 hours, of steady-state response.

7.2.2 Restoring Characteristics

For the coupled and uncoupled models to behave similarly, the restoring characteristics, i.e. the system mooring stiffness, must be similar. This is due to the non-linearity of the characteristics, and the coupling between mean, WF motion, and LF motion. A more detailed discussion on these coupling effects may be seen in Section 2.2.3. In practice however, full equality in the restoring characteristics is difficult to achieve, as SIMO and RIFLEX obtains these from different calculation procedures. For instance, RIFLEX does not include bottom friction when establishing the line characteristics, as SIMO does. For this reason, bottom friction is not included in either model. In addition, there will be small differences in pre-tension caused by numerical procedures in the software. As a result,

these two models will "operate" in different parts of their non-linear restoring characteristic, causing additional differences in both mean response and dynamic behaviour. The line characteristics are calculated by SIMO in the uncoupled model, and by RIFLEX in the coupled model.

SIMO, and hence the uncoupled model, calculates the line characteristics quasi-statically, which excludes drag forces on the line. The uncoupled characteristics are therefore independent of current. In the coupled model, however, the finite element formulation in RIFLEX allows the inclusion of current forces on the lines.

The restoring characteristics with and without base case current profile, as well as with the alternative current profile, are presented in Figures 7.1a, 7.1b and 7.2. These restoring characteristics are calculated without the effect of bottom friction. The characteristics are shown to be virtually identical in the case of no current, while an increasing discrepancy is observed as the current forces increases. The restoring calculated in RIFLEX is seen to yield a larger offset than the restoring characteristics calculated in SIMO, for a given environmental force. This is in agreement with what is seen in Section 2.6.4, and with what was observed by Ormberg and Larsen (2004). Wind and wave forces are not included in the calculation of restoring characteristics.

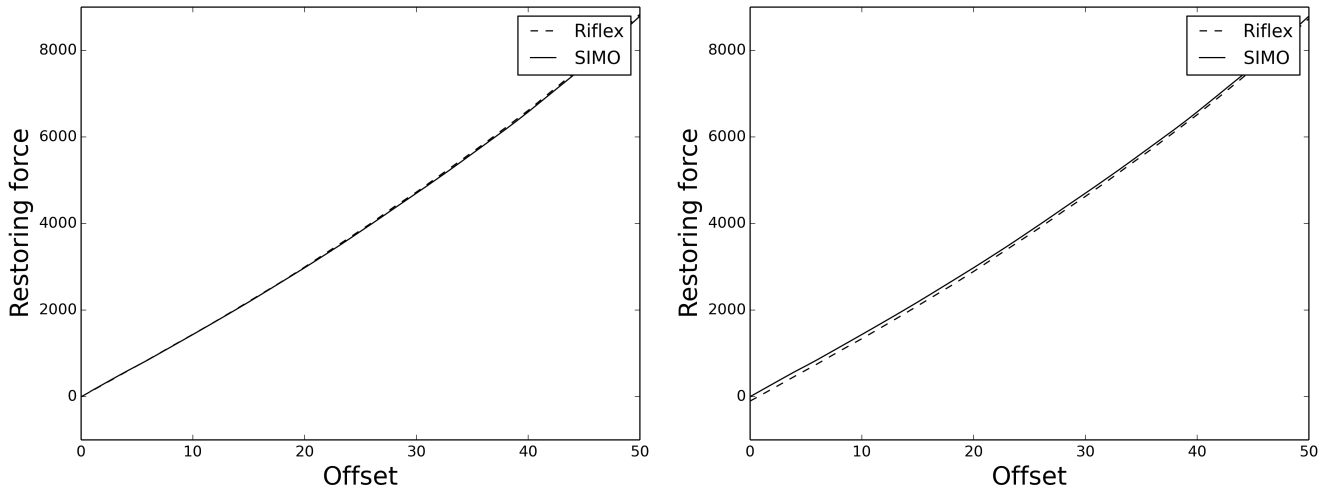

(a) Without current **(b)** With base case current profile

Figure 7.1: Restoring characteristics without and with base case current, no bottom friction

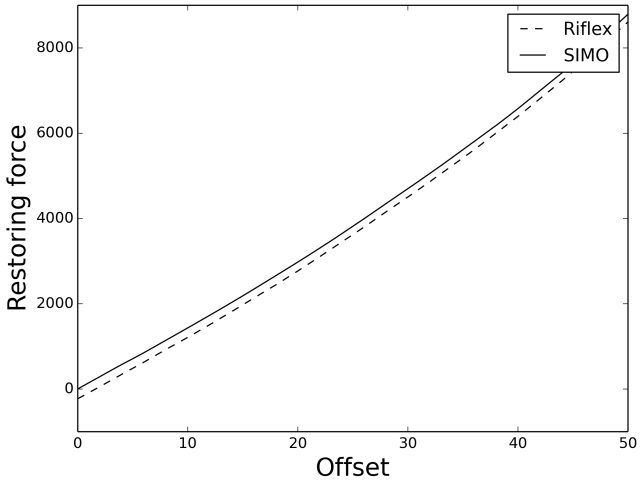

Figure 7.2: Restoring characteristics for alternative current profile, no bottom friction

In the alternative Hs/Tp, and in the alternative heading cases, as well as in the damping sensitivity study, the line and restoring characteristics are the same as that of the base case.

7.3 Base Case

This section contains the results from the base case simulations. The environmental conditions related to the cases are seen in Table 5.5.

First, results for a single seed are presented. Coupled and uncoupled results are compared and discussed in connection to the damping estimate, model limitations, and vessel response characteristics. The responses are separated into their mean, WF and LF contributions in order to study the relationship between the damping estimate and these components. Some extreme value statistics are also discussed.

Secondly, results from a seed variation are presented. Statistics of damping estimates and responses from 20 seeds are presented in order to assess the uncertainties in the damping and statistical parameters obtained from the simulations. The connection between the uncertainty in the damping estimate and the effect the responses are also discussed.

7.3.1 Vessel Offset, Single Seed

Single seed analysis is performed with seed equal to 1 for both wind and waves. The damping estimated from this analysis is:

$$B_{11} = \quad 667.7 \text{ kNs/m} \quad \text{for seed=1}$$

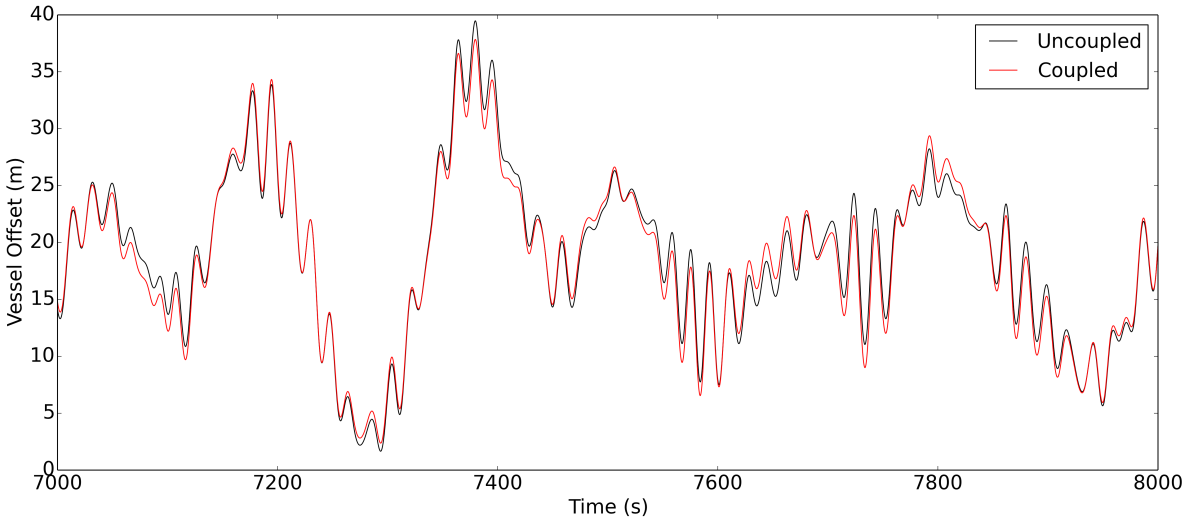

Figure 7.3: Vessel offset from initial position, base case

Figure 7.3, shows a small portion of the offset timeseries calculated for a single seed, by coupled and uncoupled analysis, when exposed to base case conditions. A fairly good match is observed, with slight differences between coupled and uncoupled vessel offset. The time series may be separated into mean, WF and LF contributions, as illustrated in Figures 7.4 and 7.5, and analysed. The corresponding statistics are presented in Table 7.1.

The mean offset show only small differences between coupled and uncoupled model, which may be attributed to a discrepancy in the restoring characteristics, and that current forces are only included in an approximate manner. The mean results seem to indicate that the method for estimating the mean current force do indeed provide a good approximation for the given condition.

From these separated figures and statistics one may observe that the uncoupled analysis is able to capture the WF motion with better accuracy than the LF motion. LF motion is resonant and will therefore be more sensitive to damping.

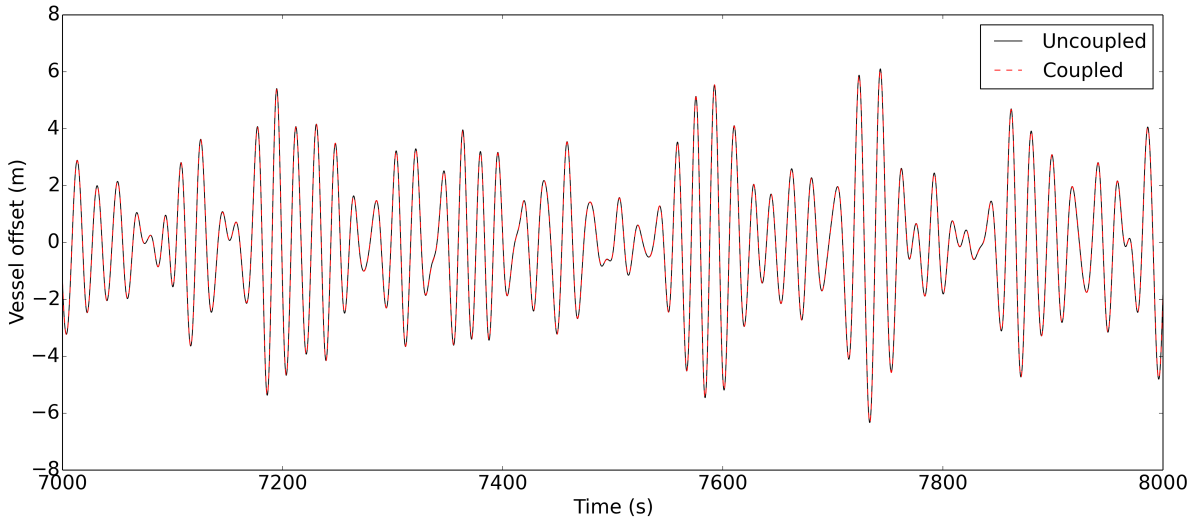

Figure 7.4: WF vessel offset from initial position, base case

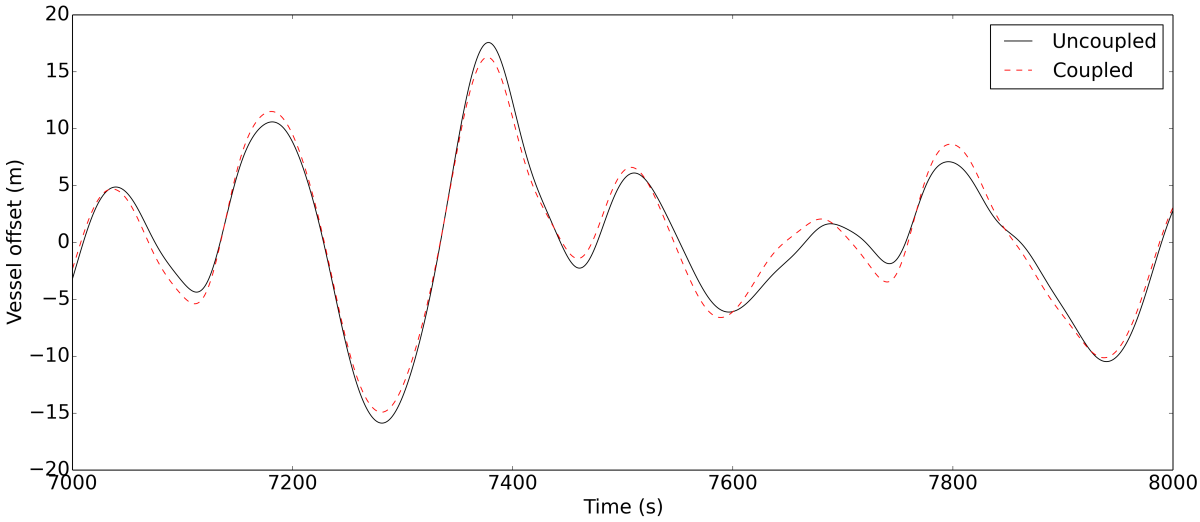

Figure 7.5: LF vessel offset from initial position, base case

The LF motion is also generally seen to be larger than the WF motion.

The uncoupled model uses a linear coefficient to represent the damping in the mooring lines, while in the coupled model the correct non-linear damping contributions from the lines are automatically included. This effect will be the main reason for the difference between coupled and uncoupled LF motions.

Because of a larger LF motion in the uncoupled model the total maximum will be larger as well. The total standard deviation in the uncoupled model is governed by the LF standard deviation, and will therefore also be larger in this model. Consequently, an accurate estimate of the mooring line damping may be crucial for the maximum offset, and ultimately the maximum tension.

Table 7.1: Vessel offset and line tension statistics for base case single seed

	Coupled					Uncoupled				
	Mean	σ^{WF}	σ^{LF}	σ^{Tot}	Max	Mean	σ^{WF}	σ^{LF}	σ^{Tot}	Max
Offset (m)	18.5	2.1	6.42	6.71	42.8	18.7	2.1	6.83	7.10	43.3
Tension (kN)	1861	117	291	312	3229	1876	119	312	334	3262

In addition to differences in the LF motion along the global x-axis, there will be some deviations in yaw motion, as indicated by Figure 7.6. These deviations will enhance the inaccuracies in the vessel offset as the two vessel models will have different projected area exposed to the environmental forces.

From the yaw time series one may also observe a phase difference, which is caused by the automatic inclusion of line damping and inertia in the coupled model. In the uncoupled model, inertia in the lines are neglected while damping is only included in an approximate manner.

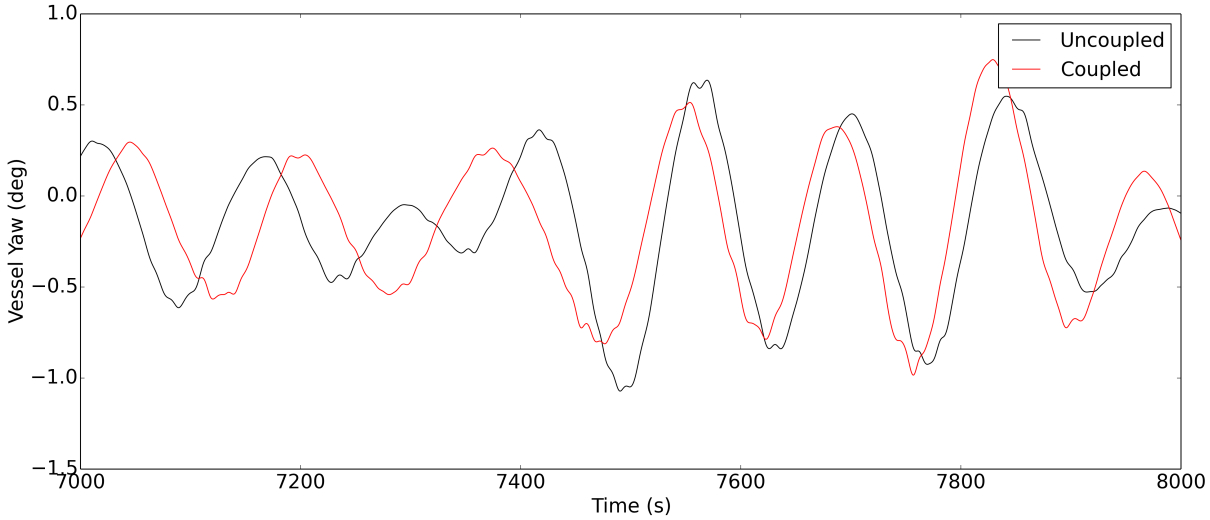

Figure 7.6: Vessel yaw motion

7.3.2 Line Tension, Single Seed

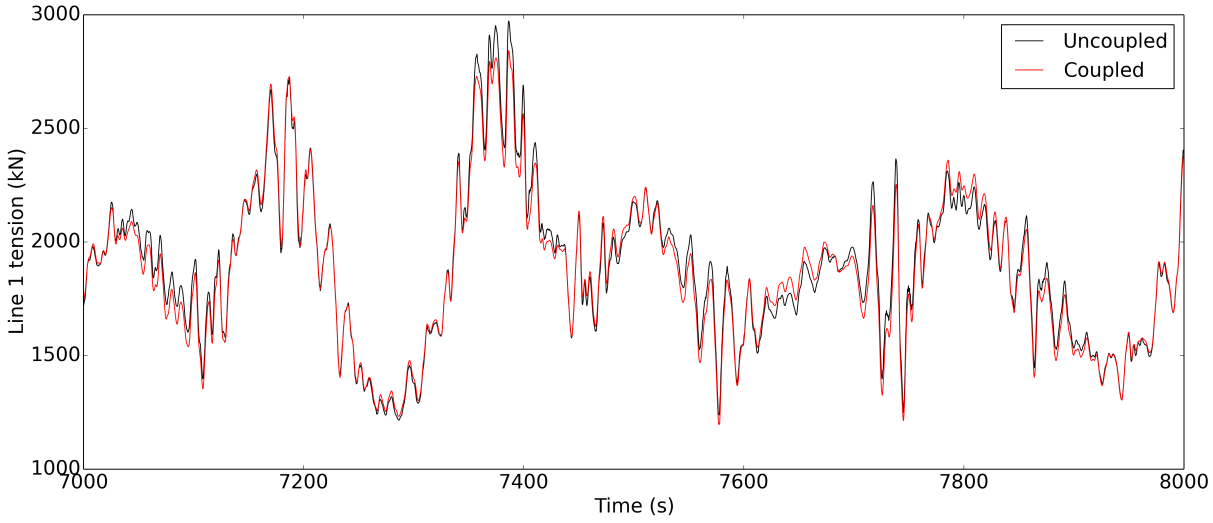

Figure 7.7: Local tension in line 1, base case

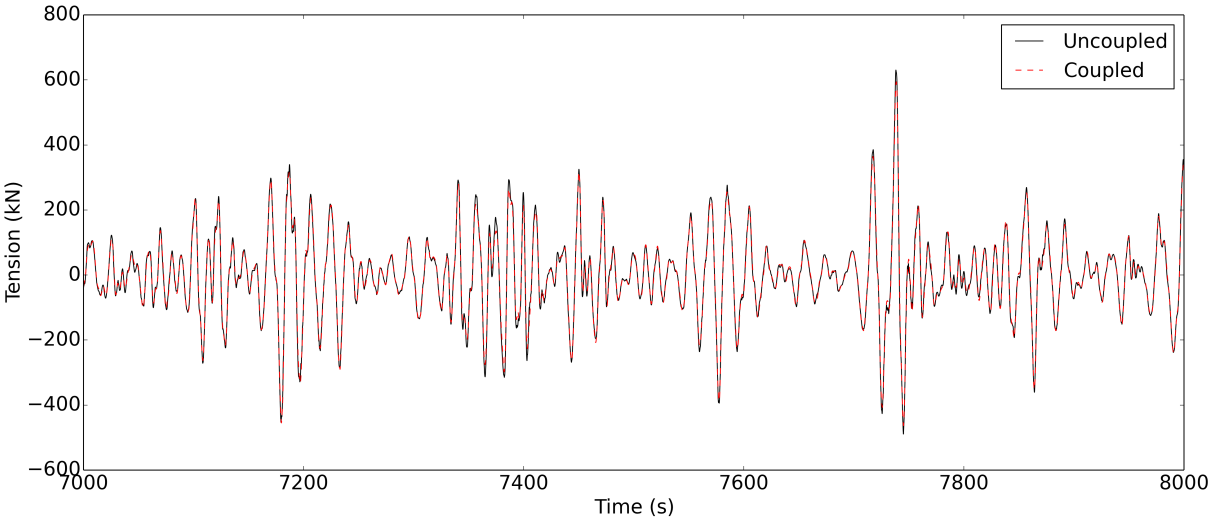

Figure 7.8: WF local tension in most loaded line 1, base case

Time series of tension in the most loaded line is seen in Figures 7.7, 7.8 and 7.9. Like vessel offset, the line tension shows small deviations between coupled and uncoupled model. In addition to the discussion related to vessel offset, the non-linearity of the line characteristics, as well as sway, heave and pitch motion will

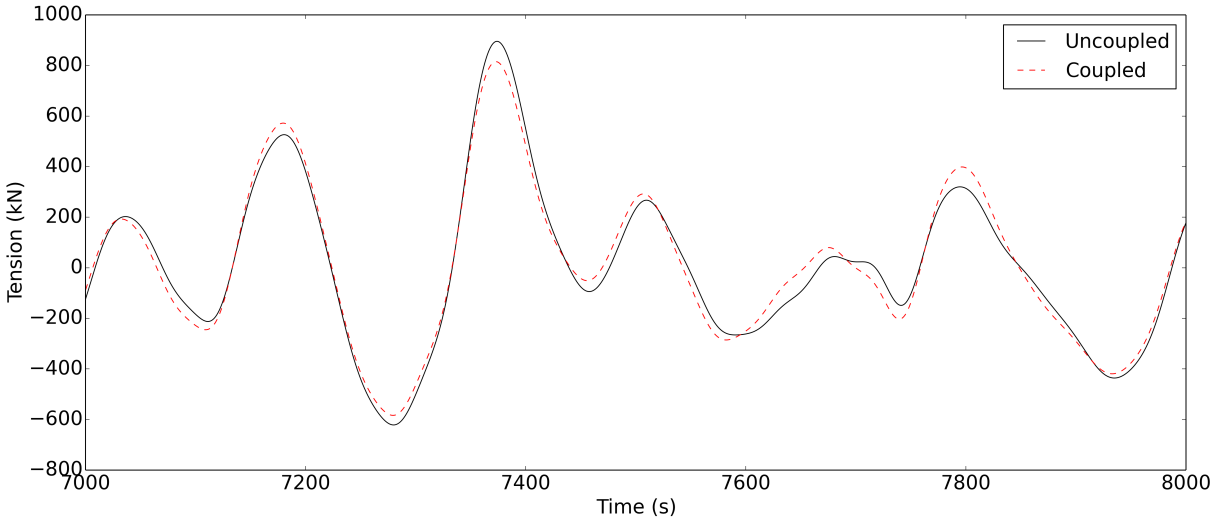

Figure 7.9: LF local tension in most line 1, base case

contribute to the total line tension. Sway, heave and pitch are important as the tension depends on the total distance between the anchor and the top end. The combination of surge, heave and pitch may cause much larger WF excitations at the top node, than one obtains by only considering the surge motion. This is explained in the discussion related to Figure 2.4. Larger WF excitation will also lead to more mooring line damping, as WF motion is the main driving force for this type of damping. Non-linearity in the line characteristics may cause additional differences in the tension. This effect will be most prominent at the peaks, since the stiffness gradient is higher for larger offsets. The effect is however quite subtle as the curvature of the line characteristics were seen to be low (see Figure 7.10).

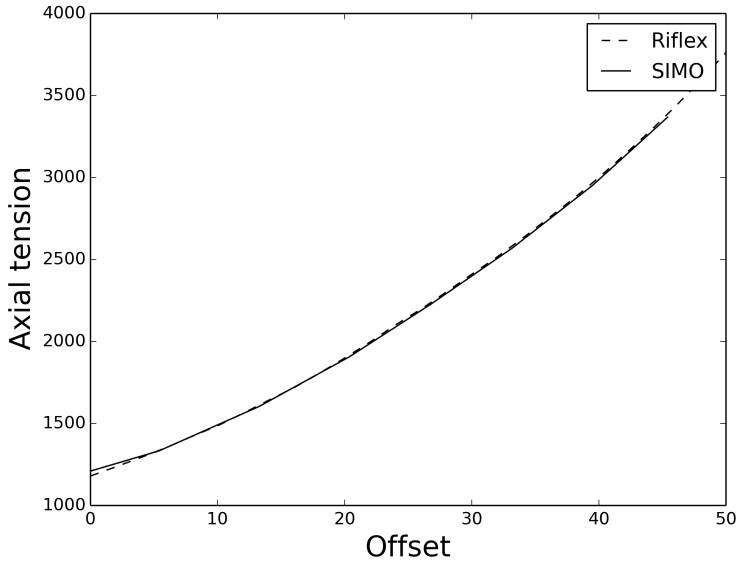

Figure 7.10: Line characteristics during base case conditions

7.3.3 Base Case, Seed Variation

As described in section 6.1.1, the line damping coefficients are estimated from coupled analyses. These damping estimates will inevitably be associated with some statistical uncertainty, and in order to assess this uncertainty, the simulation time was increased by means of a seed variation. A total of 20 sets of seeding numbers were used, corresponding to 60 hours of simulation time. From the seed variation the statistical parameters of the damping estimates, seen in Table 7.2, were found.

Table 7.2: Statistical parameters of linear damping estimate in surge from 20 seeds

	Mean	σ	Min.	Max.	CV (%)
B_{11} (kNs/m)	651.5	15.1	623.5	681.5	2.3

where CV is the coefficient of variation given by CV = σ/mean, and represents the dispersion of the estimates. From the table it is seen that the damping estimates have a low dispersion around the mean, with a coefficient of variation of only 2.3%. In addition, both the maximum and minimum estimate are within 5% of the mean. This may indicate that a large number of seeds may not be necessary in order to get a good estimate of the damping. However, the effect

of this uncertainty on the responses is system dependent, so such a conclusion should be accompanied by an assessment of the damping sensitivity.

Statistics of mean, LF and total responses are presented in Tables 7.3 and 7.4. The same differences between coupled and uncoupled analysis as in Table 7.1 are observed. The underlying mechanisms between these differences are therefore the same as the ones discussed previously. The standard deviation of WF responses have been omitted as WF motion were shown to have a small relative contribution to the total offset, and because they were shown to have a very low sensitivity to the damping estimates. The maximum LF responses are instead considered, as this will provide a better basis for assessing total extreme offset.

A low dispersion is seen in the mean offset and tension, for both coupled and uncoupled analysis. The LF responses however, are shown to have more scattered results. This is seen in the coefficient of variation (CV) for the LF standard deviation, and in particular the LF max. A CV of 2.3 % in the damping estimate is associated with a CV for the LF offset standard deviation of 6.8 % and 7.0 %, for coupled and uncoupled model, respectively. For LF max these numbers are 17.5 % and 18.1 %. It is important to note that the uncertainty in LF responses lies not only in the sensitivity of the damping, but also in the inherent statistical uncertainty associated with these responses. The latter uncertainty arises from a low number of motion cycles during a simulation, and the stochastic nature of the simulation.

Table 7.3 also show the offset standard deviations from 20 simulations. There, the LF max and total maximum are seen to be closely related. At the same time, the CV for LF maximum is seen to be much larger than the CV for total maximum. This is due to the large contribution from mean offset, which will reduce the impact on the total maximum.

From the above discussion, it is evident that the LF responses are indeed highly sensitive to the damping estimates. This sensitivity causes large uncertainty in the LF response. The damping sensitivity is further investigated in Section 7.4.4.

The Tables 7.3 and 7.4 indicate that an uncoupled analysis, using linear damping estimates and constant mean current forces obtained as previously explained, will lead to conservative estimates of LF response and total maximum. However, investigations of additional configurations and seeds are required to draw any general conclusions, in particular in connection with maximum values.

Table 7.3: Statistical parameters of coupled and uncoupled vessel offset from 20 seeds

	Coupled					Uncoupled				
	Mean	σ^{LF}	LF max	σ^{Tot}	Max	Mean	σ^{LF}	LF max	σ^{Tot}	Max
Average (m)	18.5	6.3	21.9	6.6	43.4	18.8	6.7	23.0	7.1	46.1
Std (m)	0.1	0.4	3.8	0.4	3.9	0.1	0.5	4.1	0.4	4.8
Max (m)	18.6	7.2	31.4	7.5	52.2	18.9	7.8	32.9	8.0	56.9
CV (%)	0.4	6.8	17.5	5.9	8.9	0.4	7.0	18.1	5.9	10.4

Table 7.4: Statistical parameters of coupled and uncoupled tension from 20 seeds

	Coupled					Uncoupled				
	Mean	σ^{LF}	LF max	σ^{Tot}	Max	Mean	σ^{LF}	LF max	σ^{Tot}	Max
Average (kN)	1862	287	662	309	3511	1877	307	714	333	3686
Std (kN)	3.5	20	74	18.5	386	3.8	22	75	19.1	454
Max (kN)	1868	326	901	346	4419	1885	353	945	374	4643
CV (%)	0.4	7.1	11.1	6.0	11.0	0.2	7.1	10.5	5.7	12.3

Consider the coupled results in Table 7.4. The standard deviation for extreme tension (386 kN) is seen to be much larger than the standard deviation of LF max tension (74 kN). This is due to dynamic effects from WF motion on the mooring line stiffness. As it was shown in Section 2.6.5, the stiffness depends on the excitation frequency, and a high excitation frequency will cause a higher stiffness than what is given by the quasi-static solution. This effect may contribute to very large tension spikes, induced by the WF motion, when the instantaneous offset is large. The same effect is seen in the uncoupled results.

From the extreme values based on 20 simulation, an extreme value distribution may be established. The method is described in Section 2.7.1, and the cumulative probability plotted on Gumbel papers are shown in Figures 7.11a and 7.11b. The expected mean, which is located roughly at the 57 %-quantile, is indicated on the vertical axis. The lines going through the data points are the regression lines from a least square fit. These were shown to give a much better fit to the sample, than the moment estimators. The uncoupled model is seen to overestimate the extremes, compared to the uncoupled model. In the case of a long term extreme assessment, one would typically go to an artificially high probability to account for short term variability. In such cases, the 90 %-quantile is often used, which is seen to be overestimated by the uncoupled model. The coupled model will in this case give an extreme offset around 50 m, whereas the uncoupled model

will for the same case give an extreme offset around 54 m. However, 20 seeds will generally provide too few sample points for proper extreme value estimation. The same trend is seen in the extreme tension distribution.

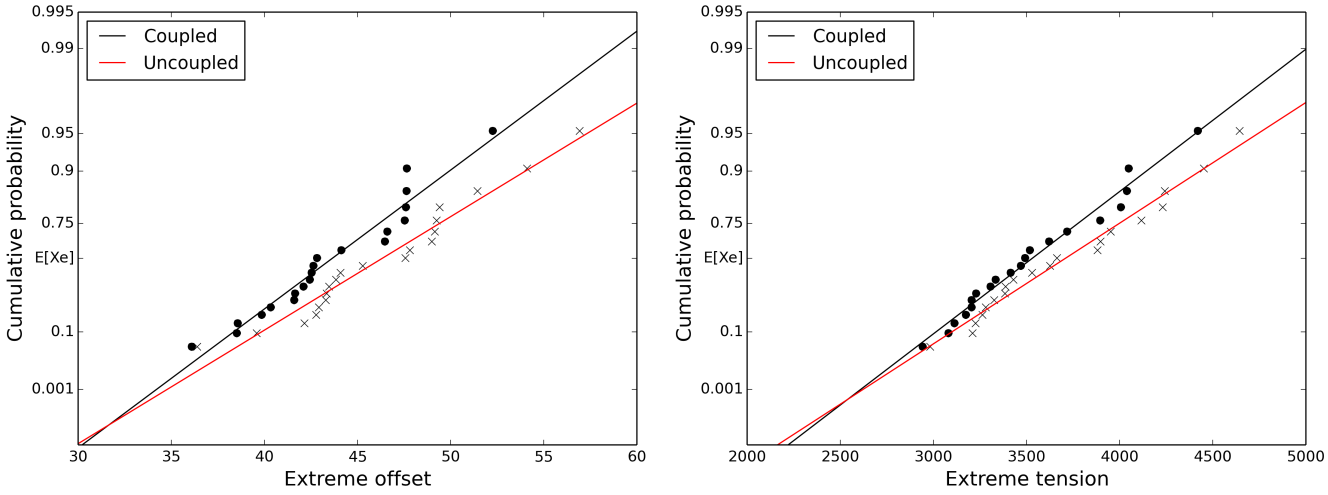

(a) Cumulative probability of extreme offset **(b)** Cumulative probability of extreme tension

Figure 7.11: Cumulative probability of extreme offset and tension

7.4 Parameter Study

In addition to the base case, the following cases are investigated:

- Alternative current profile (single seed)
- Alternative (reduced) Hs and Tp (20 seeds)
- Alternative heading with base case conditions (single seed)
- Damping sensitivity study with 0.1, 0.5 and 2.0 fractions of the damping coefficient estimated in the base case (single seed)

An alternative current profile and the damping sensitivity is investigated for a single seed as they utilize the same surface realization as the base case. An alternative Hs and Tp, however, will alter the wave spectrum, and in turn the surface realization. A direct comparison will therefore introduce large statistical uncertainty. For this reason, a seed variation is performed for alternative Hs and

Tp, using the same seed numbers as in the base case.

Using an alternative heading will lead to a different excitation of the vessel, and hence a direct comparison of responses are not performed. The focus is instead on the damping estimate only.

A summary of the environmental conditions used in the base case and the parameter studies is seen in Table 5.5

7.4.1 Alternative Current Profile

This case has the same environmental conditions as the base case, except for a different current profile. The current velocity at the sea floor is 0.5 m/s, and the profile increases linearly to 0.9 m/s at the surface. The current force on the hull will remain unchanged as the surface velocity is used on the whole vessel.

First, the results from alternative current profile and base case are compared with regards to the damping estimate and coupled responses. The standard deviation for WF offset were found to be practically independent of current and model, with a value of 2.1 for all analyses. In addition, the relative contribution of this WF motion were found to be of less importance, compared to the mean and LF offset. WF standard deviation is therefore omitted from the results.

Secondly, a comparison of uncoupled results is presented and related to the model capabilities.

Lastly, the differences between coupled and uncoupled results for base case and alternative current profile is presented, to assess whether an increase in current drag alters the difference between these respective models.

7.4.1.1 Damping Estimate

The damping estimate increases with increasing current velocity, as seen in Table 7.5, since the relative velocity between the water particles and the mooring line is larger. This creates, as drag forces are proportional to relative velocity squared, a larger coupling term in Eq. (3.2), which acts against the motion direction.

Table 7.5: Damping estimates in single seed

Case	B11 (kNs/m)	Diff. (%)
Base case	667.68	-
Alternative current	686.39	2.8

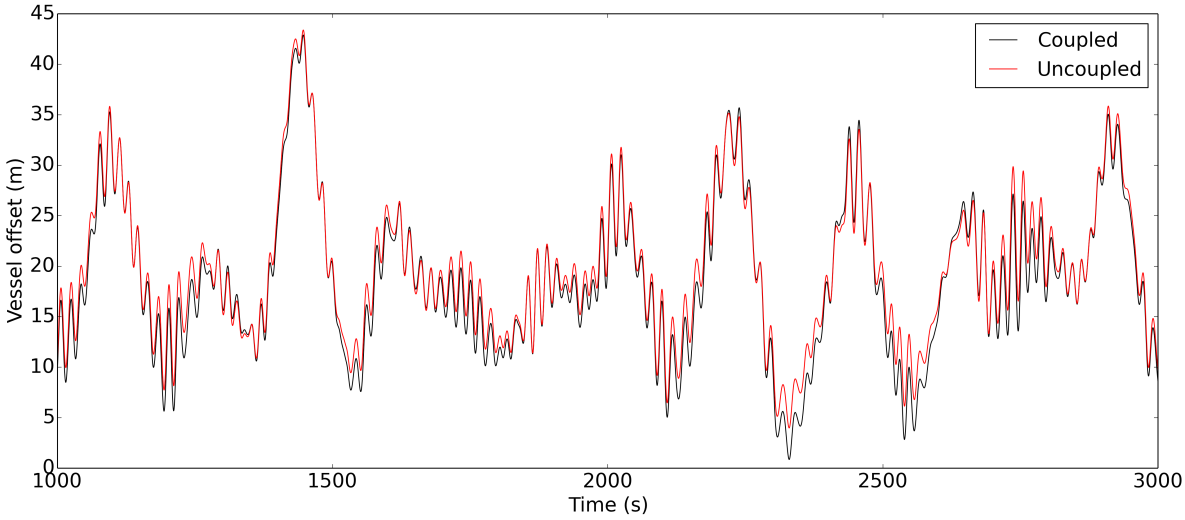

Figure 7.12: Vessel offset from initial position, alternative current profile

7.4.1.2 Coupled Results

The alternative current profile yield a higher coupled mean offset and tension than the base case. This is natural as the mean current force is much larger. The increase in mean offset means that the stiffness is higher. This will, in combination with a higher damping level, lead to less LF motion, and in turn, less total motion. The coupled maximum will be governed by the increased mean and the reduced LF motion. Consequently, only a small difference in coupled maximum is observed between base case and the alternative current profile.

Whether the coupled maximum will generally increase as a results of a larger current is difficult to predict, as the mean and the LF motion seems to have opposite relationships to the increased current. A general conclusion may therefore not be drawn from this, as the results largely depends on these relative contributions. The relative importance may in turn may be influenced by several factors, such as water depth and slender configurations. The results may therefore be purely coincidental for this particular system. From the discussion related to Tables 7.3 and 7.4, it was also found that the LF max, and in turn the total maximum, was

associated with large uncertainties. As only a single seed is used for comparison between base case and alternative current profile, it is uncertain how the change in current profile will affect the uncertainty of the LF response, and whether seed number will affect the difference in LF response between base case and current profile.

7.4.1.3 Uncoupled Results

As expected, the uncoupled results for alternative current profile are virtually identical to the base case. This may be attributed to the fact that current forces on the lines are only included in an approximate manner as a constant force acting on the vessel, and that the current velocity at the surface remains unchanged. The latter meaning the current forces on the hull are not altered. Any differences may be attributed to a difference in the mean current force from the lines.

7.4.1.4 Coupled vs. Uncoupled Results

The difference between the coupled and the uncoupled mean is larger for the alternative current profile than the base case. This is seen in both offset and tension. Its may be attributed to a larger mean current force on the lines, and to an increased discrepancy in the restoring characteristics, seen in Figures 7.1b and 7.2.

The standard deviations of total offset and tension, in Tables 7.6 and 7.7, is seen to be larger for the uncoupled model, indicating more dynamic motion. By separating the responses into their WF and LF contribution one may observe that the difference lies within the LF contribution. This is, as previously mentioned, natural as the LF responses are more sensitive to damping estimates. WF was seen to be unaffected, and is therefore ommited from the results. It was also previously mentioned that the uncoupled model uses a linear coefficient to represent the damping in the mooring lines, while the coupled model automatically includes the correct non-linear damping contributions. A larger damping level, created by more current drag on the lines, will increase the difference from this effect. The difference between coupled and uncoupled LF offset is therefore bigger in the alternative current case. This is seen by a difference of 0.4 and 0.6 in the standard deviation for LF offset, for base case and alternative current, respectively.

Table 7.6: Offset statistics for base case and alternative current profile

	Coupled					Uncoupled				
	Mean	σ^{LF}	LF max	σ^{Tot}	Max	Mean	σ^{LF}	LF max	σ^{Tot}	Max
Base case (m)	18.5	6.4	23.3	6.7	42.8	18.7	6.8	23.3	7.1	43.3
Alt. current (m)	19.3	6.2	22.9	6.5	43.2	18.8	6.8	23.3	7.1	43.2

Table 7.7: Tension statistics for base case and alternative current profile

	Coupled					Uncoupled				
	Mean	σ^{LF}	LF max	σ^{Tot}	Max	Mean	σ^{LF}	LF max	σ^{Tot}	Max
Base case (kN)	1861	291	1256	312	3229	1876	312	1270	334	3262
Alt. current (kN)	1923	288	1258	314	3300	1879	310	1267	332	3258

7.4.2 Alternative Hs and Tp

In this section, the results from a less severe 100 year storm is presented and compared to the base case. The significant wave height is reduced to 12 m, and the spectral peak period to 12.5 s. All other parameters are equal to the base case.

First, the statistics for the damping estimates, due to a seed variation with 20 seeds, are presented and discussed. The focus is on the connection between the damping estimate and the WF and LF responses.

Secondly, the response statistics are studied and explained through vessel response characteristics and damping estimates. The purpose is to study the effect of wave height and peak period on WF and LF responses.

The mooring line damping in Table 7.8 is lower for the case with alternative Hs and Tp, than for the base case. This is both because there is less WF motion on the vessel, and because the relative velocity between line element and water particle is lower, leading to lower drag. Note that drag is only taken into account in the coupled model. The reduction in WF motion may be explained by the first order transfer functions, as illustrated in Figure 7.13a . The WF response is seen to decrease as the wave period decreases. Similar trends are seen in heave and pitch, which may also be important for the total WF excitation.

Table 7.8: Damping estimates from seed variation

Case	Average (kNs/m)	Average diff. (%)	Std (kNs/m)	Max	Min	CV (%)
Base case	667.7	-	15.5	684.5	623.5	2.4
Alt. Hs, Tp	631.3	-4,15	17.0	671.5	598.7	2.7

As discussed in Section 3.4, drag will cause both an excitation and damping force. This drag damping on the mooring lines are mainly governed by WF motion, as the relative velocity between water particle and line element from this excitation mode is larger than it is for LF motion.

The coefficient of variance (CV) for the damping estimate is practically equal for the base case and alternative Hs/Tp case. The difference in CV is much lower than the CV itself, which may mean that any discrepancies may simply be due to statistical uncertainty. This indicates that the statistical uncertainty of the damping estimates is not significantly influenced by the damping level, or the magnitude of the WF and LF excitation. However, a larger seed variation, and an investigation of several cases is required before such a conclusion may be drawn.

Table 7.9: Offset statistics for base case and alternative Hs and Tp (average values)

	Coupled					Uncoupled				
	Mean	σ^{WF}	σ^{LF}	σ^{Tot}	Max	Mean	σ^{WF}	σ^{LF}	σ^{Tot}	Max
Base case (m)	18.5	2.1	6.3	6.6	43.4	18.8	2.1	6.7	7.1	46.1
Alt. Hs,Tp (m)	19.2	0.8	8.3	8.3	48.4	19.8	0.8	8.4	8.5	50.1

Table 7.10: Tension statistics for base case and alternative Hs and Tp (average values)

	Coupled					Uncoupled				
	Mean	σ^{WF}	σ^{LF}	σ^{Tot}	Max	Mean	σ^{WF}	σ^{LF}	σ^{Tot}	Max
Base case (kN)	1862	118	283	309	3511	1877	121	303	333	3686
Alt. Hs,Tp (kN)	1905	72	381	389	3784	1929	74	391	403	3946

Mean, max and the standard deviation of total offset are seen to increase in Tables 7.9 and 7.10, as Hs and Tp is reduced. By considering the WF and LF components one may observe that the former decreases while the latter increases. The standard deviation of the LF offset is, as mentioned, governed by the drift coefficients and the energy of the wave spectrum. The drift coefficients will yield larger excitations at lower periods, while the first order transfer functions will become smaller. This may be seen by Figure 7.13.

In addition, the wave energy spectrum is proportional to the significant wave height and to the square of the peak period. Hence, a reduction in these parameters will reduce the total energy in the spectrum, leading to smaller excitation forces. The total response will therefore be the result of a combination of the first order transfer functions and the wave spectrum for WF response, and the drift coefficients and the wave spectrum for LF response. It is important to note that the LF motion is due to an excitation at or near the natural periods, and hence only a low excitation force is necessary.

The damping level will also affect the LF response, as have been previously shown. Since the mooring line damping is driven by WF excitation, a reduction in WF motion will indirectly cause an increase in LF motion. Larger drift coefficient will also lead to larger mean drift forces, which are important contributions to the total mean. As the difference in motion between the base case and alternative Hs/Tp is significant, one may also assume that there will be a larger setdown effect prohibiting an increase in mean offset. However, this effect is usually more subtle than the effect of an increased mean force.

From the above discussion one may expect the mean to be larger in the case with alternative Hs and Tp than in the base case, which is confirmed by the results in Tables 7.9 and 7.10. WF responses are observed to be smaller due to less energy in the wave spectrum, but more importantly a large decrease in the first order transfer function. LF response increases with more than 30 % due to a much larger portion of the wave spectrum within LF excitation range. The effect of less total energy in the wave spectrum is outweighed by the large increase in drift coefficient, as observed in Figure 7.13b.

Table 7.11: Percentile differences between coupled and uncoupled offset

	Mean	σ^{WF}	σ^{LF}	σ^{tot}	Max
Base case	1.6	0.0	6.3	7.6	6.2
Alt. Hs, Tp	3.1	0.0	0.0	2.4	3.5

Table 7.12: Percentile differences between coupled and uncoupled tension

	Mean	σ^{WF}	σ^{LF}	σ^{tot}	Max
Base case (%)	0.8	2.5	7.1	7.8	5.0
Alt. Hs, Tp (%)	1.3	2.8	2.6	3.6	4.3

Tables 7.11 and 7.12 show the percentile differences between coupled and un-

coupled analysis. The differences in LF and total standard deviations are shown to be larger for the base case than they are for the alternative Hs and Tp case. For offset these are 7.1 % and 7.8 %, respectively in the base case, while for the alternative Hs and Tp the same values are 2.6 % and 3.6 %. WF standard deviation however, show an approximately equal discrepancy in base case and the alternative Hs and Tp case. This is an opposite effect of what was seen in the alternative current case. By reducing the damping level, the error made by introducing a linear damping coefficient is reduced. A better agreement between coupled and uncoupled is therefore achieved.

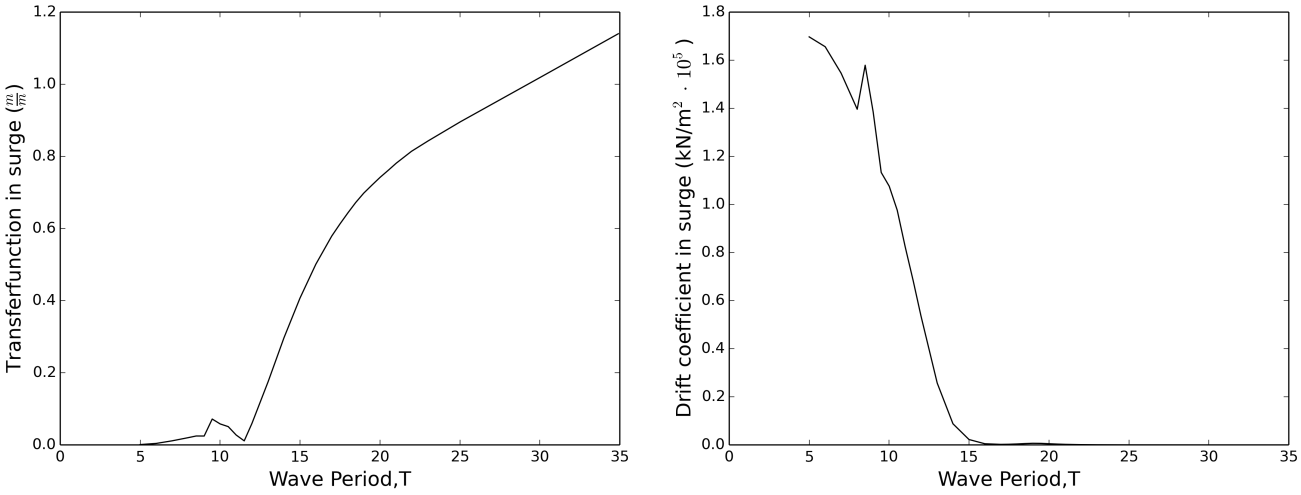

(a) First order transfer function in surge **(b)** Drift coefficient in surge

Figure 7.13: First order transfer function and drift coefficient in surge

7.4.3 Alternative Heading

An alternative heading of 15°, with environmental condition identical to the base case is investigated in order to study the effect on the damping estimate. Offset and line tension can not be directly compared, due to a difference in excitation. One should keep in mind that the damping coefficient refers to a local vessel surge motion, which for these two cases refers to different headings.

A larger heading yields a larger damping estimate (Table 7.13) since there has been an increase in WF excitation, which is the main driving force of mooring line damping. The WF excitation has increased because a larger area of the hull is exposed to the incoming waves, wind and current. This in turn, increases both

Table 7.13: Damping estimate for base case and alternative heading, single seed

Case	B11 (kNs/m)	Diff. (%)
Base case	667.7	-
Alternative heading	697.5	4.5

sway, heave, pitch and yaw, which will all contribute to displacement of the top nodes of the mooring lines. Heave and pitch will be particularly important, due to the coupling with surge motion, and because these WF motions will have a large influence on the excitation of the top nodes. Sway and yaw will contribute indirectly through the LF motion in these directions, and through the non-linear stiffness characteristic. This will in turn influence the WF response in surge, heave and pitch. A more detailed description of the coupling from LF to WF response is presented in Section 2.2.3.

7.4.4 Damping Sensitivity

In the previous result sections the damping estimates have shown to have a low dispersion about the average value. In order to get a more complete picture of the uncertainty associated with the damping estimates, and the effect on vessel and mooring line responses, an assessment of damping sensitivity is performed. Three damping fractions, 0.1, 0.5 and 2.0 of the damping estimate in the single seed base case, were arbitrarily chosen with the purpose of covering a wide range. Offset and tension results from uncoupled analysis, with various damping fraction relative to base case, are here investigated and discussed.

One should keep in mind during the discussion that the mooring line damping in sway and yaw, as well as the coupling terms between sway and yaw, are given as functions of the surge damping. This may be seen from Eq. (6.5). However, inspection showed that the contribution from these degrees of freedom to the surge response were comparatively small.

The duration of the transient response generally depends on the damping level. This may be illustrated by considering a damped forced oscillation on a system with one degree of freedom, as shown in Appendix D. Based on visual inspection of the offset time series for all damping fractions, a transient duration of 3000 seconds was chosen. This leaves 8000 seconds, or about 2.2 hours, of steady-state response. The results below refers to these 8000 seconds.

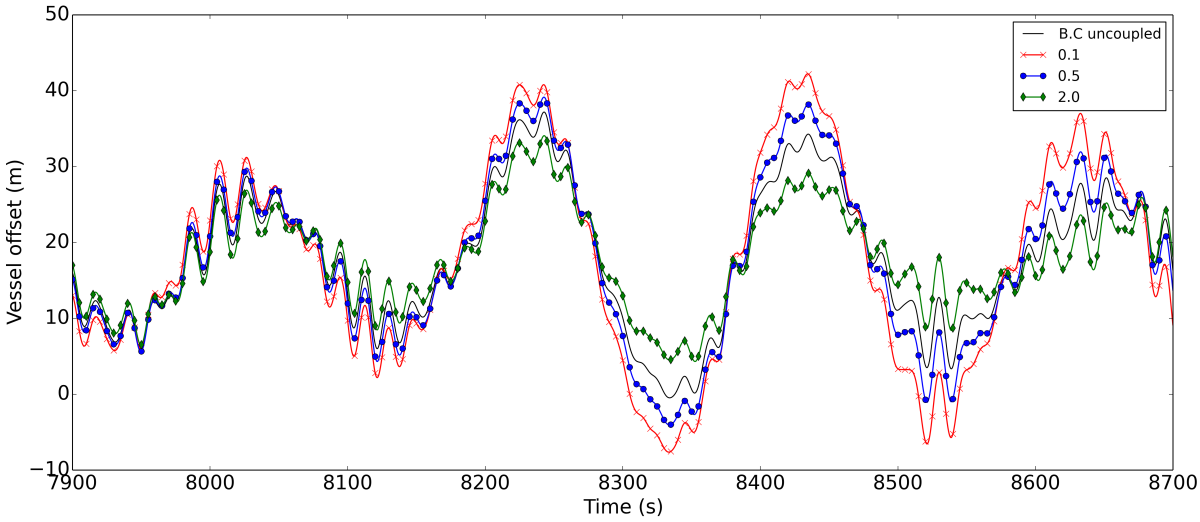

Figure 7.14: Uncoupled vessel offset for various damping fractions

Figure 7.14 presents a small portion of the time series containing the uncoupled offset for the investigated damping fractions. The notation 'B.C' in the figure refers to the damping estimate obtained for a single seed with base case conditions. Damping fractions are relative to this estimate. In the figure, the largest deviations are seen at the peaks.

Table 7.14: Uncoupled offset and line tension for various damping fractions

	Offset (m)				Tension (kN)			
Fraction	Mean	σ^{LF}	LF max	Max	Mean	σ^{LF}	LF max	Max
1.0	18.6	6.8	17.7	40.3	1875	307	900	3089
0.1	18.3	10.2	23.4	46.0	1887	453	1246	3638
0.5	18.5	8.2	19.9	43.4	1878	367	1026	3339
2.0	18.8	5.3	15.1	36.3	1874	242	758	3037

The results from the damping sensitivity study is presented in Table 7.14. WF responses have been omitted as they were found to be unaffected by the damping estimate, and because their contribution to the total response was relatively low. The results are also presented as percentile differences relative to base case in Table 7.15, in order to better assess their sensitivity to the damping estimate.

As all environment conditions remains constant throughout the sensitivity study, the difference in mean is purely due to a varying setdown effect, caused by the non-linear stiffness. This is seen in the negative correlation with the LF standard deviation. The setdown effect is small for this system, and hence there are only small variations in mean.

The LF responses are seen to be highly sensitive to the damping estimate. A reduction of 50 % in the damping estimate leads to an increase in LF standard deviation of 21% for the offset. For lower levels of damping the sensitivity is greater. This can be seen by that a further reduction in damping leads to a larger difference in LF standard deviation. The LF responses are also very sensitive to an increase in damping, although to a lesser extent. This is in agreement with previous observations (Langen and Sigbjornsson, 1979), which states the effectiveness of a damping increase on a resonant motion reduces for increasing damping level. This is illustrated in Figure 7.15 (Langen and Sigbjornsson, 1979) by the effect on the dynamic amplification factor (DAF). Increase of 100 % in the damping estimate has the same effect on the LF standard deviation as a reduction of 50 %, in terms of magnitude.

LF max response follows much of the same trend as the LF standard deviation, although the effect is less pronounced. The reason for a smaller effect on the maximum LF response is partially due to a higher stiffness at large offsets.

Since LF max is less sensitive than the overall LF motion, and since LF motion only constitutes a part of the total offset, the sensitivity of total maximum is limited. A reduction of 50 % in the damping estimate corresponds only to an increase of 8 % in the maximum offset and tension. This indicates that an accurate estimate of the damping is vital for a good representation of the LF response, but not necessarily so for the total response. However, this largely depends on the systems configurations, such as water depth, mooring line geometry, pre-tension, etc. A multitude of simulations will still be necessary in order to reduce the statistical uncertainty.

In section 7.4.2, the maximum and minimum damping values for base case and alternative Hs and Tp were seen to be within 7 % of the mean estimate. In the above discussion the mean and maximum responses were seen to be little and moderately sensitive to a change in damping estimate within the investigated range. LF response, and in particular the LF standard deviation was seen to be very sensitive within the investigated range. However, an investigation of the sensitivity within smaller deviations from the mean, say within 10 % of the mean might reveal that the LF responses are not significantly influenced in this range.

Table 7.15: Percentile difference as a function of damping fraction

	Offset diff. (%)				Tension diff. (%)			
Fraction	Mean	σ^{LF}	LF max	Max	Mean	σ^{LF}	LF max	Max
0.1	-2	50	32	14	1	48	38	18
0.5	-1	21	12	8	0	20	14	8
2.0	1	-22	-15	-10	0	-21	-16	-2

Such a conclusion may indicate that only a few simulations are necessary for sufficient accuracy of the LF responses as well.

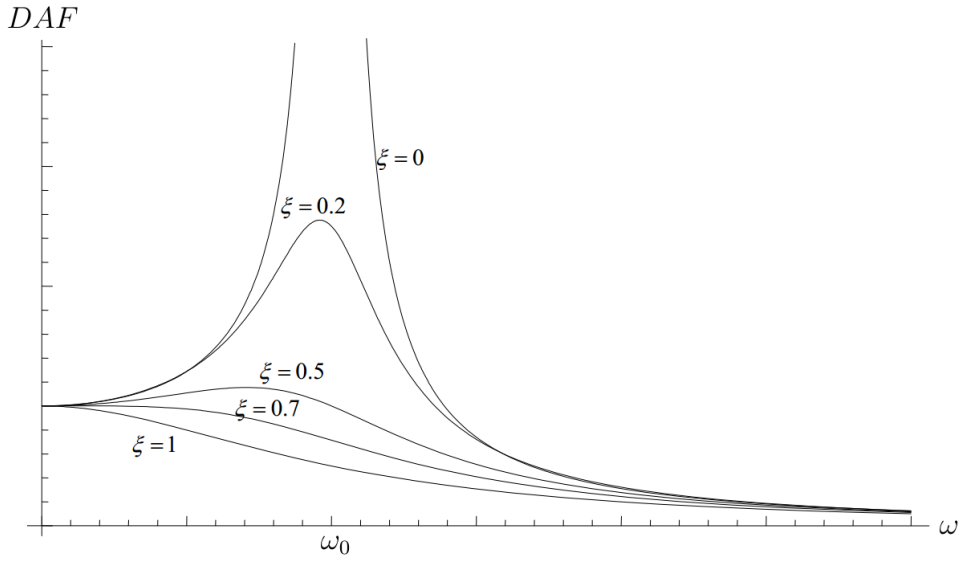

Figure 7.15: The effect of changing damping levels on the dynamic amplification factor (DAF)

Chapter 8
Concluding Remarks

The base case results show that the damping estimation technique provides a good agreement between coupled and uncoupled simulation, for the given conditions. The WF motion is practically identical for the coupled and the uncoupled model. LF motion on the other hand, is a resonant motion and will therefore be more sensitive to the damping estimate. Consequently, there are slight differences between coupled and uncoupled LF responses. The total response will be a combination of mean, WF and LF responses, and the sensitivity of the extreme response to the damping estimate will very much depend on the relative importance of the LF motion. This in turn, will depend on factors such as spectral peak period and current velocity/profile.

From a seed variation with base case conditions, it was shown that a low uncertainty in the damping estimates may lead to moderate or large uncertainty in the LF responses and, by consequence, in the total response. The conclusion was enhanced by the damping sensitivity study. This confirms the sensitivity of damping in the LF response, and shows that this may be important for total response as well. Therefore, accurate uncoupled response estimates requires an even more accurate damping estimate. This might for example be achieved from a larger number of seed variations, longer coupled simulations, or a better estimation procedure.

Increasing the current causes a larger relative velocity between line segment and water particles, which leads to more damping in the mooring lines. However, an increase in current have a minimal effect on the uncoupled results as the current forces are only included in an approximate manner. The coupled results are seen to yield larger mean, as well as lower WF and LF response, compared to base case conditions. This shows that the inaccuracy in the uncoupled model increases with current velocity.

The reduction in peak period and wave height resulted in a lower damping esti-

mate. The damping was lowered due to a decrease in WF excitation, the main driving force for the damping estimate. A lowering of the spectral peak period generally increases the LF response and lowers the WF response. This may be explained by the opposite trends in the drift coefficients and the first order transfer functions, respectively. A lowering of the peak period and wave height will also reduce the energy in the wave spectrum, which will enhance the reduction of WF excitation. For LF motion, the increasing drift coefficient outweighs the reduction in spectral energy. A reduction in WF motion will also contribute to an increase in LF motion, through the mooring line damping.

The linear damping coefficient estimated from a coupled analysis were seen to provide a good agreement between coupled and uncoupled results, for the most moderate conditions. As the damping level in the mooring lines increases, the limitations in using such a linear coefficient becomes more apparent. Great care should therefore be taken when using an approximate representation of the mooring line damping in areas with large currents or significant WF excitation.

Alternative heading causes an increase in damping due to a larger exposed are of the hull, which in turn give rise to larger WF excitation forces.

A damping sensitivity showed that mean and WF responses were not sensitive to the damping estimate, whereas LF response was highly sensitive. The sensitivity of the total response will depend on the relative importance of LF response.

Chapter 9
Recommendation for further work

During the damping sensitivity study a rather wide range of damping fraction were investigated, while the actual damping estimates were seen to be closely scattered around the mean. This resulted in a rather crude assessment, which could only give overall conclusions about the sensitivity. To better assess the effect of the uncertainty in the damping estimates, a more narrow range of estimates should be investigated. This could typically be $\pm 2\sigma$ from the mean, or between the maximum and minimum estimate. Such an investigation may show that the low frequency and maximum components of the responses are only slightly or moderately affected within the range of damping estimates. If so, the criteria of required simulations in a seed variation may be relaxed. However, this will depend on the purpose of the analysis.

The case studies have been performed without bottom friction. Including bottom friction will alter the line characteristics, and consequently the restoring characteristics. This is likely to reduce the damping estimate, as the bottom friction will restrict the vessel motion.

Alternative methods for damping estimation should be investigated with the purpose of improving the applicability of a simplified uncoupled analysis.

The analyses have been performed by the use stochastic phase and deterministic amplitudes. This will have a tendency to underestimate to response for extreme conditions, such as the ones investigated in the study. The effect on the damping estimate is uncertain, but as the estimate is based on a mean square approach it is suspected to be moderate. However, in combination with other damping estimation techniques, this could prove to be important.

It was suggested in the discussion that the uncertainty in the damping estimates was not significantly affected by the damping level, or the magnitude of the wave-frequency and low-frequency motion. A larger variation of seed numbers should

be used in order to conclude on whether uncertainty in damping estimates is indeed independent on the damping level and environmental condition. Several cases will need to be investigated to conclude on the effect of environmental condition, e.g. various current profiles.

The water depth was remained fixed during the case studies. Previous observations in the literature suggest that the importance of mooring line forces on the system response increases with water depth. Similar investigations as the ones performed in this thesis should be studied in order to check if water depth alters the overall trends.

A larger range of vessel headings, as well as an assessment of the responses from these headings, would be interesting to investigate, with regards to the damping estimate and its relationship with different response components.

Bibliography

Baarholm, G. S. (2014), 'Private communication'.

Chakrabarti, S. K. (2005), *Handbook of Offshore Engineering*, Elsevier Ocean Engineering.

Faltinsen, O. M. (1998), *Sea Loads on Ships and Offshore Structures*, Cambridge University Press.

Garrett, D. (2005), 'Coupled Analysis of FLoating Production Systems', *Offshore Engineering* (32), 802–816.

Garza-Rios, L. O., Bernitsas, M. M. and Nishimoto, K. (1997), 'Catenary Mooring Lines with Nonlinear Drag and Touchdown'.

Ginsberg, J. H. (1995), *Advanced Engineering Dynamics*, Cambridge University Press.

Grue, J. (1996), 'Wave Drift Damping on Floating Bodies in Slow Yaw Motion', *Journal of Fluid Mechanics* .

Haver, S. (2014), 'TMR4195 - Design of Offshore Structures', University Lecture, Norwegian University of Science and Technology.

Haver, S. and Winterstein, S. R. (2008), 'Environmental Contour Lines: A Method for Estimating Long Term Extremes by a Short Analysis', *SMTC-067-2008* (68).

Kaasen, K. E., Lie, H. and Mo, K. (2007), *MIMOSA User's Documentation, Program version 6.3-06*, Marintek, Trondheim, Norway.

Kleiven, G. and Haver, S. (2004), 'Met-Ocean Contour Lines for Design; Correction for Omitted Variability in the Response Process', *International Offshore and Polar Engineering Conference* .

Langen, I. and Sigbjornsson, R. (1979), *Dynamisk analyse av konstruksjoner*, Tapir.

Larsen, C. M. (2012), *TMR4182 Dynamisk Analyse av Konstruksjoner*, Tapir.

Larsen, C. M. (2013), 'Private communication'.

Leira, B. (2010), *Probabilistic Modelling and Estimation*, Tapir.

Leonard, J. W. (1987), *Tension Strutures: Behaviour and Analysis*, McGraw-Hill.

Lie, H. (2013), 'TMR7 - Experimental Methods in Marine Hydrodynamics', University Lecture, Marintek.

Lone, E. N. (2009), 'Stochastic Analysis of Anchor Line Forces For FPU', M.Sc Thesis. Norwegian University of Science and Technology.

Low, Y. and Langley, R. (2007), 'Time and Frequency Domain Coupled Analysis of Deepwater Floating Production Systems', *Applied Ocean Research* .

Low, Y. and Langley, R. (2008*a*), 'A Hybrid Time/Frequency Domain Approach for Efficient Coupled Analysis of Vessel/mooring/riser Dynamics', *Journal of Offshore Mechanics and Arctic Engineering (OMAE)* .

Low, Y. and Langley, R. (2008*b*), 'Understanding the Dynamic Coupling Effects in Deep Water Floating Structures Using a Simplified Model', *Ocean Engineering* .

Magnussen, E. (2013), 'Analysis and Design of Mooring Lines for Floating Production Units.', Project Thesis. Norwegian University of Science and Technology . *Unpublished*.

Matsui, T. (1986), 'Analysis of Slowly Varying Wave Drift Forces on Compliant Structures', *Proceedings of the fifth International Offshore Mechanics and Arctic Engineering Symposium (OMAE), Tokyo, Japan* pp. 289–296.

Myrhaug, D. (2005), *Statistics of Narrowband Processes and Equivalent Linearization*, Tapir.

Nilsen, K. R. (2007), 'Alternative Methods for Analysis of Motion and Line Forces for Drilling Platforms', M.Sc. Thesis. Norwegian University of Science and Technology.

Næss, A. and Moan, T. (2013), *Stochastic Dynamics of Marine Structures*, Cambridge University Press.

Nygaard, E. and Eik, K. J. (2004), 'Asgard Metocean Design Basis', *Statoil Report, PTT-NKG-RA 0055, Rev. 4* .

Ormberg, H., Fylling, I., Larsen, K. and Sodahl, N. (1997), 'Coupled Analysis of Vessel Motions and Mooring and Riser System Dynamics', *Proceedings of the International Conference on Offshore Mechanics and Arctic Engineering - OMAE, vol. I-A* pp. 91–110.

Ormberg, H. and Larsen, K. (2004), 'Coupled Analysis of Floater Motion and Mooring Dynamics for a Turret-Moored Ship', *Applied Ocean Research* .

Ormberg, H., Sodahl, N. and Steinkjer, O. (1998), 'Efficient analysis of mooring systems using de-coupled and coupled analysis', *Proceedings of the International Conference on Offshore Mechanics and Arctic Engineering - OMAE* .

Rodenbusch, G., Garrett, D. and Anderson, S. (1986), 'Statistical Linearization of Velocity-Squared Drag Forces', *Proceedings of OMAE'86, Tokyo* pp. 123–139.

Sødahl, N. R. (1991), 'Methods for Design and Analysis of Flexible Riser', Ph.D Thesis. Norwegian University of Science and Technology.

SIMO project team (2012), *SIMO - Theory Manual Version 4.0 rev. 1*, Marintek, Trondheim, Norway.

van den Boom, H. (1985), 'Dynamic Behaviour of Mooring Lines', *Behaviour of Offshore Structures* .

Webster, W. C. (1994), 'Mooring-Induced Damping', *Ocean Engineering* .

Wichers, J. and van Sluijs, M. (1982), 'On the Low-frequency Surge Motions of Vessels Moored in High Seas', *Proceedings of the 14th Annual Offshore Tecnhology Conference (OTC)* .

Appendix A

Coordinate systems and Conversions

All coordinate systems used are right-handed cartesian systems with clockwise rotations defined as positive. Quadratic wind and current coefficient are imported from a MOSSI file, which uses a different coordinate system than SIMO and Riflex. In both systems the x- and y-axis describe the horizontal directions with the x-axis pointing in the same global direction. However, while SIMO and Riflex has the z-axis pointing upwards, the MOSSI file format has it pointing downward, as shown in figure A.1.

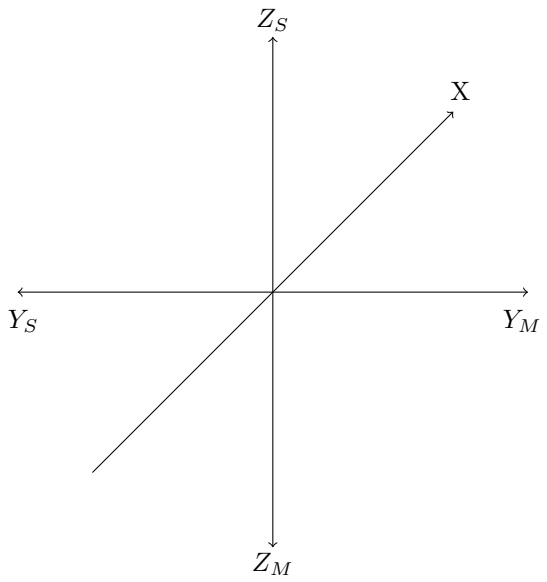

Figure A.1: Coordinate systems in MOSSI and SIMO/RIFLEX

In addition, two different ways of defining environmental directions are used: (i) "comming from" which denotes propagation towards the origin, and (ii) "propagation", which is the opposite. Table A.1 describes the conventions for environmental directions.

Table A.1: Description of axis system and environmental directions

Format	**Directions of z-axis**	**Wind and waves**	**Current**
MOSSI	Downward	Comming from	Propagation
SIMO/RIFLEX	Upward	Propagation	Propagation

Table A.2: Conversion of environmental directions, MOSSI to SIMO/RIFLEX

Current	**Wind/waves**
360 - α	180 - α

Due to the difference in definitions of environmental directions, it is necessary to convert the wind and current coefficients. The proper conversion scheme is shown in table A.2, where α denotes the direction in MOSSI format. An illustration of the angular differences are also shown for current in figure A.2. In the case of wind or waves, the difference may be illustrated by having the environmental arrow in SIMO/RIFLEX placed as in the figure, and the environmental arrow for MOSSI mirrored about the origin pointing inwards.

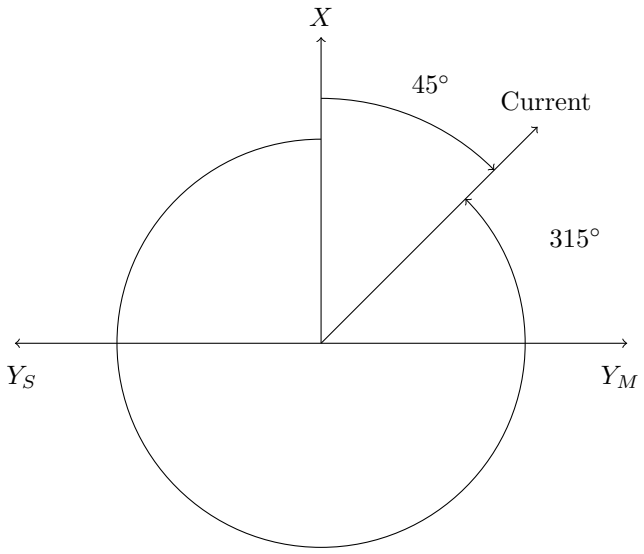

Figure A.2: Illustration of difference in environmental directions

Appendix B
Analysis Strategy

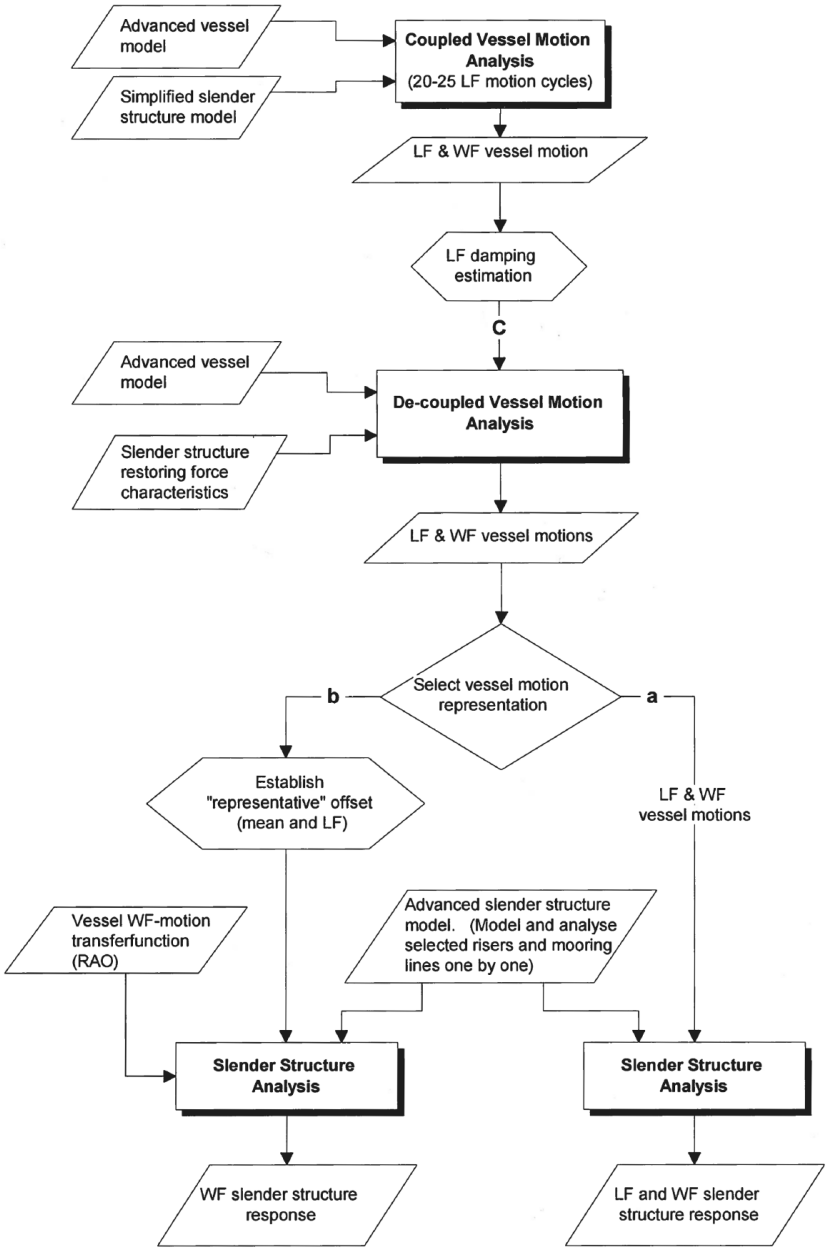

Figure B.1: Analysis strategy with linear damping estimates

Appendix C
Change of reference system

C.1 Conventional Method

The transformation from a globally fixed reference system to a local one that follows the body orientation is commonly performed by the use of a rotation matrix. The rotation matrix is defined by the sequence in which the incremental rotations are performed. For a body-fixed transformation this sequence is $\Delta\theta_x \rightarrow \Delta\theta_y \rightarrow \Delta\theta_z$, where the rotations represent roll, pitch and yaw, respectively. It can be shown that for positive rotations defined as clockwise when looking from the origin, this yields the rotation matrix (Ginsberg, 1995):

$$T = \begin{bmatrix} C_y Cz & C_x S_z + S_x S_y C_z & S_x S_z - C_x S_y C_z \\ -C_y S_z & C_x C_z - S_x S_y S_z & S_x C_z + C_x S_y S_z \\ S_y & -S_x C_y & C_x C_y \end{bmatrix}$$

where S and C denotes the sine and cosine, and the subscripts x, y and z denotes the rotation about these respective axes, e.g. $S_x = \mathbf{sin}\Delta\theta_x$.

The position of a point represented in the local body-fixed reference system $\mathbf{x}$ can be obtained from the known position in the globally fixed system $\mathbf{X}$, the rotation matrix $\mathbf{T}$ and the distance between the local and the global system $\mathbf{v}$ as:

$$\mathbf{x} = \mathbf{T} \cdot \mathbf{X} + \mathbf{v}$$

During a time domain simulation this rotation matrix will need to be updated for each time step.

C.2 Dummy Line Approach

As each row in the rotation matrix represent the unit vector for the dof i expressed in global coordinates, i.e. row 1 represent the local x-axis, one can use an alternative approach for establishing these without the need of rotation angles.

$$\mathbf{T} = \begin{bmatrix} \mathbf{n}_{x_L} \\ \mathbf{n}_{y_L} \\ \mathbf{n}_{z_L} \end{bmatrix} \tag{C.1}$$

where $\mathbf{n}_{i_L}$ is the unit vector of local axis i expressed in global coordinates.

The approach involves connecting dummy lines of unit length along the local axes of the vessel with one node at the origin. This way the difference in global position of the ends will represent the unit vector for that particular local axis expressed in global coordinates. These unit vectors can then be put directly into the rotation matrix. As the axes are orthogonal the third vector may be found from the cross product of the other two. For this reason, dummy lines were only placed along the x- and y-axes.

C.3 Line Forces and Surge Motion

Since the goal is to find a damping estimate which refers to the local vessel system, both the vessel motion and mooring line forces must be transformed to this common reference system.

The relationship between the global earth-fixed and the local line reference system can be expressed as:

$$\mathbf{X}_{line} = \mathbf{T}_1 \cdot \mathbf{X}_{global} \tag{C.2}$$

Likewise, the relationship between the global earth-fixed and the local vessel reference system can be expressed as:

$$\mathbf{X}_{vessel} = \mathbf{T}_2 \cdot \mathbf{X}_{global} \tag{C.3}$$

From this we obtain:

$$\mathbf{X}_{vessel} = \mathbf{T}_2 \cdot \mathbf{T}_1^{-1} \cdot \mathbf{X}_{line} \tag{C.4}$$

and because $\mathbf{T}_1$ is an orthogonal matrix:

$$\mathbf{X}_{vessel} = \mathbf{T}_2 \cdot \mathbf{T}_1^{T} \cdot \mathbf{X}_{line} \tag{C.5}$$

where $\mathbf{T}_1$ and $\mathbf{T}_2$ are rotation matrices between the respective reference systems. $\mathbf{T}_1$ is given as output by RIFLEX, whereas $\mathbf{T}_2$ is established from unit vectors of the dummy lines, as shown in Eq. (C.1) .

The vectors $\mathbf{X}$ may represent either force or position. When calculating local position, the whole $\mathbf{T}_1$ matrix must be utilized, whereas since mooring lines are modelled as bar elements with zero shear forces, the force in local vessel system simplifies to:

$$\begin{bmatrix} F_x \\ F_y \\ F_z \end{bmatrix}_{local} = \begin{bmatrix} \mathbf{n}_{x_L} \\ \mathbf{n}_{y_L} \\ \mathbf{n}_{z_L} \end{bmatrix}_2 \cdot \begin{bmatrix} T_{11} & T_{12} & T_{13} \\ T_{21} & T_{22} & T_{23} \\ T_{31} & T_{32} & T_{33} \end{bmatrix}_1^T \cdot \begin{bmatrix} T_e \\ S_y = 0 \\ S_z = 0 \end{bmatrix} = \begin{bmatrix} \mathbf{n}_{x_L} \\ \mathbf{n}_{y_L} \\ \mathbf{n}_{z_L} \end{bmatrix}_2 \cdot \begin{bmatrix} T_{11} \\ T_{12} \\ T_{13} \end{bmatrix}_1 \cdot T_e \tag{C.6}$$

where T_e denotes the local axial tension. Equation (C.6) must be solved for each mooring line and summed in order to get the total force contribution.

The vessel position expressed in local vessel coordinates is simply found from equation (C.3).

Appendix D
Damped Forced Oscillation

The duration of the transient response generally depends on the damping level. This may be illustrated by considering a damped forced oscillation on a system with one degree of freedom:

$$m\ddot{u} + c\dot{u} + ku = R(t) \tag{D.1}$$

For a harmonic excitation, the transient part of the solution to an under critically damped system may be given as (Larsen, 2012):

$$u_p(t) = e^{-\gamma\omega_0 t} A\sin(\omega_d t) = \bar{u}_p(t)\sin(\omega_d t) \tag{D.2}$$

where ω_0 and ω_d are the free and damped eigenfrequencies, respectively, A is an integration constant given by the initial conditions, $\bar{u}_p$ is the amplitude of the transient response, and γ is the damping level given as:

$$\gamma = \frac{c}{2m\omega_0} \tag{D.3}$$

The exponential term in Eq. (D.2) describes the decay of the transient motion. The ratio, r, describing the relationship between two transient amplitudes is seen to have the following proportionality :

$$r = \frac{\bar{u}_{p,i}(t)}{\bar{u}_{p,BC}(t)} \propto \frac{e^{c_i/2m\omega_0}}{e^{c_{BC}/2m\omega_0}} \tag{D.4}$$

where c_{BC} denotes the damping estimated in the base case, and c_i the damping estimate for a different damping fraction. Consequently the ratio of the transient amplitudes become:

$$r \propto e^{f_i - 1} \tag{D.5}$$

where f_i denotes the damping fraction, and is given as $c_i = f_i \cdot c_{BC}$. From Eqs. (D.4) and (D.5) is evident that large damping fractions prolongs the decay time of the transient response.

Appendix E

Damping Estimation Code

This section contains the main code used to estimate the linear damping coefficient in surge. The programming language is python 2.7 and requires the numpy and matplotlib libraries. Both the python distribution and the additional libraries should be 32 bit distributions. This script, along with a matlab code for Monte-Carlo simulations, is attached to an enclosed memory stick (see Appendix F).

```
'''''''''''''''''''''''''''''''''''''''
    File:   damping_estimation.py
    Author: Eivind T. Magnussen

    Code is based on the prosedure described by Ormberg et. al. (1998)

    Procedure is devided into:
    A. Input parameters and initiation
    1. Reading SIMO/RIFLEX result files and converting global position and
        local line forces into local vessel system
    2. Low pass filtering of the zero mean vessel position and line forces
    3. Numerical differentiation by methods of difference to obtain
        local surge velocity. (Accuracy O[h^2])
    4. Calculate and write damping estimate to file

    Reference:
    Ormberg, Soedahl and Seinkjer (1998) - "Efficient analysis of mooring systems
    using de-coupled and coupled analysis", Conference on Offshore Mechanics
    and Arctic Engineering (OMAE)
'''''''''''''''''''''''''''''''''''''''


import numpy as np
import matplotlib.pyplot as plt
import matplotlib
from matplotlib.ticker import FormatStrFormatter
import linecache
from scipy import integrate
from numpy.fft import rfft, irfft#, rfftfreq
import os, sys

class dampingestimator(object):
    """docstring for dampingestimator"""
    def __init__(self):#, arg):
        super(dampingestimator, self).__init__()

    def rotmatT1(self, linenum, num, T1path):
        T = [float(elem) for elem in linecache.getline(T1path, num).split()]
        # Method for calculating line forces expressed in global coordinates.
        # Values from Riflex
        start = (linenum-1)*9+1         #First column of mooring line
        stop = linenum*9+1          #Last --"--
        T = np.array(T[start:stop])
        self.T1 = T.reshape((3,3))      #Transposed T due to file structure.

```

```
46      def rotmatT2(self, nodepath,num):
47          # Method for transforming from global to local vessel coordinates
48          # (body-fixed) by means of dummy node coordinates
49          dumx1 = np.array([float(elem) for elem in linecache.getline...
50                      (nodepath, num).split()[1:4]])
51          dumx2 = np.array([float(elem) for elem in linecache.getline...
52                      (nodepath, num).split()[4:7]])
53          dumy2 = np.array([float(elem) for elem in linecache.getline...
54                      (nodepath, num).split()[7:10]])
55          unitx = dumx2 - dumx1
56          unity = dumy2 - dumx1
57          unitz = np.cross(unitx,unity)
58          self.T2 = np.array([unitx,unity,unitz])
59
60      def locpos(self, num, motionpath):
61          # Method for transforming position from global to
62          # local vessel coordinates
63          FPSOpos = np.array([float(elem) for elem in linecache.getline...
64                      (motionpath, num).split()[1:4]])  # Global vessel position
65          self.locpos = np.dot(self.T2,FPSOpos)
66          return self.locpos[0]
67
68      def forcelocal(self, axial):
69          # Method for transforming tension from
70          # local line to local vessel coordinates
71          self.force = (self.T2.dot(self.T1)).dot([axial,0,0])
72          hlineforce = self.force[0]
73          return hlineforce
74
75      def numdiff(self, surge, time):
76          # Method for numerical differentiation by methods of differences,
77          # with accuracy of second order
78          num = len(time)
79          vel=[]       # FPSO velocity
80          for num,k in enumerate(range(len(time))):
81              if num<3:                #Forward difference for first two points.
82                  vel.append((-3*surge[k]+4*surge[k+1]-surge[k+2])/...
83                              (2*(time[k+1]-time[k])))
84              elif num >len(time)-3:  #Backward difference for last two points.
85                  vel.append((3*surge[k]-4*surge[k-1]+surge[k-2])/...
86                              (2*(time[k]-time[k-1])))
87              else:                    #Central difference on rest
88                  vel.append((surge[k+1]-surge[k-1])/(2*(time[k+1]-time[k])))
89          return vel
90
91  class filtering(object):
92      def rfftfreq(self, n, d=1.0):
93          if not (isinstance(n,int) or isinstance(n, integer)):
94              raise ValueError("n should be an integer")
95          val = 1.0/(n*d)
96          N = n//2 + 1
97          results = np.arange(0, N, dtype=int)
98          return results * val
99
100     def lp_filter(self, x, dt, T):
101         """
102         Low-pass filter.
103
104         Parameters
105         ----------
106         x : array
107             Input signal.
108         dt : float
```

```
            Time step [s].
        T : float
            Filtering period [s]. 20 s suitable for irregular wave excitation.
        """
        f_cut = 1./T
        n = x.size
        W = filt.rfftfreq(n, dt)
        f_signal = rfft(x,n)

        win = np.zeros(np.shape(W))
        win[W.__abs__()<=f_cut] = 1.

        xout = irfft(f_signal*win, n)
        return xout

''''''''''''''''''''''''''''''''''''
Main code
''''''''''''''''''''''''''''''''''''
if __name__=='__main__':
    # A. Input parameters and initiation
    xturret = [48.32,0,0] # Distance between turret center and vesel C.O.G
    #Path to folder containing SIMO/RIFLEX result files
    postpath='E:\\Eivind\\base_case\\'  # path to post processing output files
    case = 'Base case'  # Case identifier. E.g. 'Base case'

    #  Seed sets, divided into groups of 5 due to memory restrictions in Python
    A = [1,2,3,4,5]
    B = [6,7,8,10,11]       # NB: not 9, due to failed coupled analysis
    C = [12,13,14,15,16]
    D = [17,18,19,20,21]

    for seed in [1]:
        path='E:\\Eivind\\base_case\\'  # path to analysis results folder

        # Vessel position in global coordinates
        motionpath  = path+'coupled_position.res'
        # Local lineforces
        forcepath   = path+'sima_elmfor.asc'
        # Global node displacements of dummyline. Needed for T2 calculations
        nodepath    = path+'sima_noddis.asc'
        # Rotation matrix between local line and global coord
        T1path      = path+'sima_elmtra.asc'

        # Vectors containing lineforces, surge motion and damping estimate,
        # all in local vessel system
        time=[]
        Fx=[]
        surge=[]
        timestep = 0.1
        start = int(200/timestep)       # Skip first transients
        filt = filtering()              # Inititate filtering instance

        # 1. Transform forces and motions over to local vessel system
        try:
            ffile = open(forcepath,'r')
        except:
            print "Files for seed %d not found"%seed
            continue

        for num,fline in enumerate(ffile.readlines(),1):    # Each time step
            print "Seed %d, time step %d of 11000"%(seed,num)
            #print "Seed %d, time step %d of 110000"%(seed,num)
            if not fline:
```

```
                continue
            fline = fline.split()  # Local line force vector for all lines
            time.append(float(fline[0]))
            instance = dampingestimator()

            # Vessel motion
            instance.rotmatT2(nodepath,num)
            surge.append(instance.locpos(num, motionpath))

            # Total horizontal force for current time step
            hforce=[]    # Horizontal force in all lines in local vessel coord

            for linenum,fl in enumerate(fline,0): # For each mooring line
                if linenum == 0:        # If time column, then skip to next
                    continue
                # Transformation matrix between global and local line
                instance.rotmatT1(linenum,num,T1path)
                # Axial force in local vessel coord. for each line
                axialves=instance.forcelocal(float(fl))
                # Horizontal force for each line
                hforce.append(axialves)
            # Total horizontal force in vessel coord. for current time step)
            Fx.append(sum(hforce))

        ffile.close()

        # 2. Low pass filtering of zero mean line forces and surge motion
        print "2/5 Filtering"
        dt = 0.1    # Filtering sample time step
        T = 20      # Filtering cut-off period
        surge_mean=sum(surge)/len(surge)
        surge = [(elem-surge_mean) for elem in surge]
        surge = filt.lp_filter(np.array(surge), dt, T)
        Fx_mean = sum(Fx)/len(Fx)
        Fx = [(elem-Fx_mean) for elem in Fx]
        Fx = filt.lp_filter(np.array(Fx), dt, T)

        # 3. Numerical differentiation of surge
        vel = instance.numdiff(surge,time)

        # 4 Damping estimation
        # Remove transient part
        time = time[start:]
        vel = vel[start:]
        Fx = Fx[start:]

        # Calculate and write damping estimates to file
        if seed==1:
            opentype = 'w+'     # Overwrite file if seed=1
        else:
            opentype='a'        # Append if seed>1
        with open(postpath+'dampingestimates_%s.res'%case, opentype) as B11file:
            numerator = (np.dot(vel,Fx))/len(vel)
            denominator = (np.dot(vel,vel))/len(vel)
            B11 = -numerator/denominator    # Linear damping coefficient in kNs/m
            B11file.write('B11_seed'+str(seed)+': '+str(B11) +' kNs/m\n')
```

Appendix F

Attached Memory stick: Description of Content

This appendix describes the contents of the attached memory stick. A *readme.txt* file, which contains the same descriptions, is also included on the memory stick.

Analysis (Folder):
Contains input files for the coupled RIFLEX task, as well as the uncoupled SIMO and RIFLEX tasks. It also contains the workspace files *Master.sima* and *Master.stask* which contains the complete SIMA workspace with condition sets and input configurations.

damping_estimation.py
Contains the code which performs the damping estimation, based in simultaneous time series of mooring line forces and vessel position.

mone_carlo.m
The matlab code which performs the Monte-Carlo simulations, in order to establish confidence intervals for the extreme value distributions.

master_report.pdf
The final pdf file containing the master report, i.e. this document.

master_poster.pdf
Poster, which briefly describes the thesis.